

1 **Glaciers determine the sensitivity of hydrological processes to perturbed climate**  
2 **in a large mountainous basin on the Tibetan Plateau**

3

4

Yi Nan <sup>1,2</sup>, Fuqiang Tian <sup>1,2</sup>

5 **Affiliation:**

6

1. Department of Hydraulic Engineering & State Key Laboratory of Hydrosience and  
7 Engineering, Tsinghua University, Beijing 100084, China

8

2. Key Laboratory of Hydrosphere Sciences of the Ministry of Water Resources, Tsinghua  
9 University, Beijing 100084, China

10

11 **Corresponding to:** Fuqiang Tian

12

Email: [tianfq@tsinghua.edu.cn](mailto:tianfq@tsinghua.edu.cn)

13

14 **Abstract**

15

The major rivers on the Tibetan Plateau supply important freshwater resources to riparian  
16 regions, but are undergoing significant climate change in recent decades. Understanding the  
17 sensitivities of hydrological processes to climate change is important for water resource  
18 management, but large divergences exist in previous studies because of the uncertainties of  
19 hydrological models and climate projection data. Meanwhile, the spatial pattern of local  
20 hydrological sensitivities was poorly explored despite the strong heterogeneity on the Tibetan  
21 Plateau. This study adopted the climate perturbation method to analyze the hydrological  
22 sensitivities of a typical large mountainous basin (Yarlung Tsangpo River, YTR) to climate  
23 change. We utilized the tracer-aided hydrological model Tsinghua Representative Elementary  
24 Watershed-Tracer-aided version (THREW-T) to simulate the hydrological and cryospheric  
25 processes in the YTR basin. Multiple datasets and internal stations were used to validate the  
26 model, to provide confidence to the baseline simulation and the sensitivity analysis. Results  
27 indicated that: (1) The THREW-T model performed well on simulating the streamflow, snow  
28 cover area (SCA), glacier mass balance (GMB), and stream water isotope, ensuring good  
29 representation of the key cryospheric processes and a reasonable estimation of runoff

30 components. The model performed acceptably on simulating the streamflow at eight internal  
31 stations located in the mainstream and two major tributaries, indicating that the spatial pattern  
32 of hydrological processes was reflected by the model. (2) Increasing temperature led to  
33 decreasing annual runoff, smaller inter-annual variation, more even intra-annual distribution,  
34 and an earlier maximum runoff. It also influenced the runoff regime by increasing the  
35 contributions of rainfall and glacier melt overland runoff, but decreasing the subsurface runoff  
36 and snowmelt overland runoff. Increasing precipitation had the opposite effect to increasing  
37 temperature. (3) The local runoff change in response to increasing temperature varied  
38 significantly, with changing rate of -18.6% to 54.3% for 5°C of warming. The glacier area ratio  
39 (GAR) was the dominant factor of the spatial pattern of hydrological sensitivities to both  
40 perturbed temperature and precipitation. Some regions had a non-monotonic runoff change rate  
41 in response to climate perturbation, which represented the most dynamic regions within the  
42 basin, as they kept shifting between energy and water limited stages. The GAR and mean annual  
43 precipitation (MAP) of the non-monotonic regions had a linear relation, and formed the  
44 boundary of regions with different runoff trends in the GAR-MAP plot.  
45

46 **1. Introduction**

47 The Tibetan Plateau (TP), known as the “Asian Water Tower”, is the source region of  
48 several major rivers in Asia (e.g., Yarlung Tsangpo-Brahmaputra Lantsang-Mekong, Indus,  
49 Ganges). The contributions of runoff in the source regions of TP rivers to the total runoff in  
50 whole basins range from 6%-60% (Tang et al., 2019; Wang et al., 2020; Cao and Pan, 2014),  
51 sustaining the ecosystems and supplying valuable freshwater resources for downstream  
52 livelihoods (Immerzeel et al., 2010; Lutz et al., 2014). The sustainable socioeconomic  
53 development and the decision-making of water resource management in the riparian countries  
54 around the TP rely heavily on the runoff in the major river basins (Cui et al., 2023). Meanwhile,  
55 the TP is a typical high mountainous cryosphere, characterized by large stores of frozen soil  
56 and frequent multiphase water transferring, resulting in complex hydrological processes and  
57 multiple water sources including rainfall, snowmelt and glacier melt (Li et al., 2019; Yao et al.,  
58 2022). The melting processes of frozen water are determined by energy budget, and the runoff  
59 change on the TP is extremely sensitive to climate change (Gao et al., 2019). Consequently,  
60 understanding hydrological processes and estimating the runoff change on the TP is not only of  
61 great practical significance, but also a frontier scientific question in global change.

62 The TP is undergoing significant climate change in recent decades, with a warming rate  
63 twice the global average level (Yao, 2019). Based on the recently released Coupled Model  
64 Intercomparison Project Phase 6 (CMIP6) (Eyring et al., 2016), the warming levels of 1.5°C,  
65 2°C and 3°C over the TP will be attained around the 2030s, 2050s and 2070s, respectively, and  
66 the precipitation is also likely to increase significantly (Cui et al., 2023). The hydrological  
67 cycling and water resources will change correspondingly; thus it is important to understand the  
68 hydrological processes on the TP and the hydrological response to climate change. Plenty of  
69 studies have adopted hydrological models to project the runoff change on the TP in the future,  
70 but the reported trends and changing rates varied considerably in existing studies. Wang et al.  
71 (2021) and Lutz et al. (2014) projected an increasing runoff trend till the end of 21<sup>st</sup> century,  
72 while Cui et al. (2023) predicted the runoff to decrease before the 2030s and turn over to an  
73 increasing trend after that. A primary reason for the divergence in existing studies is the model  
74 uncertainties. The parameters are usually inadequately constrained solely by the streamflow  
75 observation data because of the complex hydrological processes, resulting in large uncertainties

76 in the estimation on the contributions of runoff components (Tian et al., 2020; Nan et al., 2021a),  
77 which influence the runoff projection significantly. For instance, Lutz et al. (2014) estimated  
78 the contribution of glacier melt to annual runoff as 0.86~40.59% in the major TP rivers,  
79 resulting in an increasing runoff with climate warming, while Cui et al. (2023) estimated the  
80 contribution as 0.73~14.33% and resulting in a decreasing trend in the near future. Nonetheless,  
81 recently developed hydrological models integrating key cryospheric processes (e.g., Cui et al.,  
82 2023) have been proved as effective tools for hydrological simulations on the TP, and the high-  
83 quality datasets of snow and glacier (e.g., Chen et al., 2018; Hugonnet et al., 2022) can provide  
84 adequate validation for the corresponding models. Moreover, tracer-aided hydrological models  
85 integrating modules of tracer storage, mixture, and transportation processes forced by the  
86 outputs of isotopic general circulation models (iGCMs) have proved to constrain the  
87 hydrological model uncertainties significantly (He et al., 2019; Birkel and Soulsby, 2015;  
88 Stadnyk and Holmes, 2023), especially for the separation of runoff components (Nan et al.,  
89 2021a, 2023). These developments of models and datasets bear the potential to provide a more  
90 reasonable baseline for streamflow projection.

91 Another major source of runoff projection uncertainty is the uncertainty of climatic forcing  
92 data (Li et al., 2014). The climatic data in the future are generally generated by the general  
93 circulation models (GCMs), which cannot be directly adopted in the catchment scale because  
94 of the insufficient spatial resolution and accuracy, so downscaling and bias correction are  
95 necessary steps in using GCM data at regional scale (Xu et al., 2019; Olsson et al., 2015).  
96 However, even being corrected by the observation data during the historical period, the  
97 divergence among the outputs of different GCMs is still significant. For example, the difference  
98 in the precipitation change over the TP among 22 CMIP6 products could be larger than 50%  
99 (Cui et al., 2023). Bloschl and Montanari (2010) pointed out the large uncertainties of studies  
100 analyzing the impact of climate change, and compared them to throwing a dice. As an  
101 alternative method, producing hypothesized climate change scenarios by perturbing the current  
102 temperature and precipitation data has proved to be valuable in investigating the hydrological  
103 sensitivities to climate change (Ayguen et al., 2020; Rasouli et al., 2015; He et al., 2021b). The  
104 range of climate perturbation is assumed based on the possible change range projected by an  
105 ensemble of GCMs, providing a possible runoff change range accordingly (Su et al., 2023; He

106 et al., 2021b). The climate perturbation method also allows for a deeper analysis of the separate  
107 effect of each climatic factor and the compensation effects among them (He and Pomeroy,  
108 2023).

109 Although plenty of studies have been conducted for the TP rivers to project the runoff  
110 change or analyze the hydrological sensitivities to climate change, most of them were  
111 conducted at the regional or basin scale (e.g., Su et al., 2023; Zhang et al., 2022b). The local  
112 hydrological response to climate change could significantly differ among small catchments due  
113 to the different geographical and meteorological characteristics (Bai et al., 2023), which is  
114 important for local water resources utilization and management (Zhang et al., 2015).  
115 Considering the strong heterogeneity in meteorological factors and land surface conditions in  
116 the large river basins on the TP (Wang et al., 2021; Li et al., 2020), the local hydrological  
117 sensitivities to climate change should have strong variability over the TP. However, the spatial  
118 pattern and influence factors of the local hydrological sensitivities within the basin are poorly  
119 explored, partly due to the scarce hydrological stations for model validation, resulting in a lack  
120 of confidence in the spatial representation of hydrological processes.

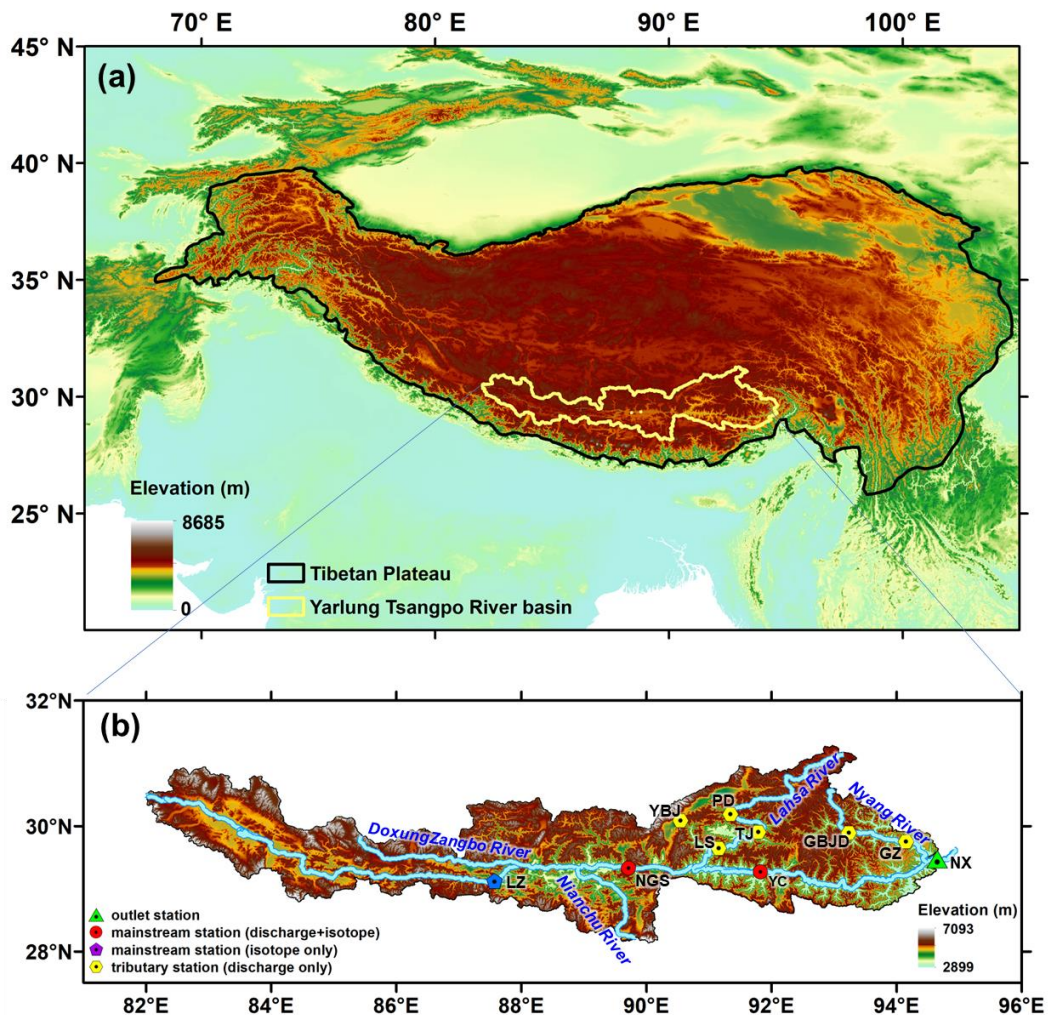
121 Motivated by the mentioned background, this study utilized the spatially distributed tracer-  
122 aided hydrological model THREW-T developed by Nan et al. (2021b) in the Yarlung Tsangpo  
123 River basin, a typical large mountainous basin on the Tibetan Plateau, to explore its  
124 hydrological sensitivity to perturbed temperature and precipitation. Snow, glacier, isotope data  
125 and observation streamflow at nine stations were collected to validate the model. The spatial  
126 pattern of the local hydrological sensitivities and the influence factors were analyzed in  
127 particular. The main objectives of this study are as follows: (1) to test the performance of  
128 THREW-T model on simulating all the hydrological and cryospheric processes in the Yarlung  
129 Tsangpo River basin, (2) to analyze the sensitivities of hydrological processes in the Yarlung  
130 Tsangpo River basin to a reasonable range of perturbed temperature and precipitation, and (3)  
131 to analyze the spatial pattern and the influence factors of the local hydrological sensitivities.

## 132 **2. Data and methodology**

### 133 **2.1 Study area**

134 This study focused on the Yarlung Tsangpo River (YTR) basin, the upstream part of the

135 Brahmaputra River basin, located in the southern TP (Figure 1). The YTR is one of the longest  
 136 rivers originating from the TP (longer than 2000 km), extending in the range of 27~32°N and  
 137 82~97°E with an elevation extent of 2900~6900 m a.s.l. (above sea level). The mean annual  
 138 precipitation and temperature in the YTR basin are around 500 mm and -0.2 °C, respectively.  
 139 The YTR has four major tributaries, i.e., DoxungZangbo, Nianchu River, Lhasa River, and  
 140 Nyang River, from upstream to downstream. The precipitation is dominated by the South Asian  
 141 monsoon in the Indian Ocean hydrosphere-atmosphere system, resulting in an obviously wet  
 142 season from June to September. The outlet hydrological station along the mainstream is the  
 143 Nuxia station, above which the drainage area is approximately  $2 \times 10^5$  km<sup>2</sup>, and around 1.5% is  
 144 covered by glaciers.



145  
 146 **Figure 1.** Locations and topography of (a) the Tibetan Plateau and (b) the Yarlung Tsangpo  
 147 River basin. The stations used for model validation are shown in Figure (b). The abbreviations

148 NX, YC, NGS, LZ, GZ, GBJD, LS, TJ, PD and YBJ represent Nuxia, Yangcun, Nugesha, Lazi,  
 149 Gengzhang, Gongbujiangda, Lhasa, Tangjia, Pangduo and Yangbajing stations, respectively.

## 150 2.2 Data

151 The 30 m resolution digital elevation model (DEM) data for the YTR basin was extracted  
 152 from the Geospatial Data Cloud (<https://www.gscloud.cn>). Daily precipitation, temperature,  
 153 and potential evapotranspiration data were extracted from the China Meteorological Forcing  
 154 Dataset (CMFD, Yang and He, 2019) with 0.1° resolution. For the cryospheric processes, the  
 155 Tibetan Plateau Snow Cover Extent (TPSCE) product (Chen et al., 2018) and the second glacier  
 156 inventory dataset of China (Liu, 2012) were adopted to denote the snow and glacier coverage.  
 157 The yearly glacier elevation change data with 0.5° resolution developed by Hugonnet et al.  
 158 (2021) was used to represent the glacier mass balance. For the underlying conditions, the  
 159 MODIS leaf area index (LAI) product MOD15A2H (Myneni et al., 2015) and normalized  
 160 difference vegetation index (NDVI) product MOD13A3 (Didan, 2015) were adopted to  
 161 represent the vegetation coverages, and the Harmonized World Soil Database (HWSD, He,  
 162 2019) was used to estimate the soil property parameters. Daily streamflow data at nine stations  
 163 were collected (Figure 1 and Table 1).

164 **Table 1.** The name, location and data period of the hydrological stations

Station	Mainstream/tributary	Period
Nuxia	Mainstream	1991~2015
Yangcun	Mainstream	2001~2010
Nugesha	Mainstream	2001~2010
Gengzhang	Nyang river	2001~2015
Lhasa	Lhasa river	2001~2015
Gongbujiangda	Nyang river	2006~2009, wet season
Yangbajing	Lhasa river	2006~2015, wet season
Pangduo	Lhasa river	2001~2015, wet season
Tangjia	Lhasa river	2001~2015, wet season

165 Grab samples of precipitation and stream water were collected in 2005 at four stations  
 166 along the mainstream of YTR, i.e., Lazi, Nugesha, Yangcun, and Nuxia, from upstream to  
 167 downstream, for isotope analysis (Table 2, Liu et al., 2007). The outputs of Scripps Global  
 168 Spectral Model with isotope incorporated (isoGSM, Yoshimura et al., 2008) with 1.875°  
 169 resolution were extracted to represent the spatiotemporal variation of precipitation isotope in  
 170 the YTR basin. According to our previous assessment based on the measurement precipitation

171 isotope data, the isoGSM captured the seasonality of precipitation isotope well, but had  
 172 systematic overestimation biases in the YTR basin, which were highly correlated to the altitude  
 173 (Nan et al., 2021a). The corrected isoGSM in the YTR basin produced by Nan et al. (2022) was  
 174 adopted in this study.

175 **Table 2.** Summary of measurement isotope data in the YTR basin during 2005

Station	Period	Precipitation			Stream		
		Number of samples	$\overline{\delta^{18}\text{O}}$ (‰)	SD (‰)	Number of samples	$\overline{\delta^{18}\text{O}}$ (‰)	SD (‰)
Nuxia	14 Mar. – 23 Oct.	86	-10.33	7.18	34	-15.74	1.60
Yangcun	17 Mar. – 5 Oct.	59	-13.17	7.10	30	-16.57	1.69
Nugesha	14 May. – 22 Oct.	45	-14.29	7.99	25	-17.84	0.99
Lazi	6 Jun. – 22 Sep.	42	-17.41	5.75	22	-16.52	1.43

### 176 2.3 The tracer-aided hydrological model

177 A distributed tracer-aided hydrological model, Tsinghua Representative Elementary  
 178 Watershed-Tracer-aided version (THREW-T) model, developed by Tian et al. (2006) and Nan  
 179 et al. (2021b), was adopted to simulate the hydrological and isotopic processes in the YTR basin.  
 180 The model uses the representative elementary watershed (REW) method for spatial  
 181 discretization of basins, dividing the whole catchment into REWs based on DEM data. Each  
 182 REW is further divided into two vertically distributed layers (i.e., surface and subsurface layers),  
 183 including eight subzones (i.e., surface layer: vegetation zone, bare zone, main channel reach  
 184 zone, sub stream network zone, snow-covered zone, and glacier-covered zone; subsurface layer:  
 185 unsaturated zone and saturated zone) (Reggiani et al., 1999; Tian et al., 2006). This study  
 186 divided the YTR basin into 297 REWs, with an average area of 694 km<sup>2</sup>, ranging from 162 to  
 187 2753 km<sup>2</sup>. More model details are provided in Tian et al. (2006).

188 A cryospheric module representing the evolutions of snowpack and glacier was  
 189 incorporated into the model for application in cold regions. The total precipitation was  
 190 partitioned into liquid and solid precipitation according to a temperature threshold, which was  
 191 set as 0°C. The degree-day factor method was used to calculate the meltwater. The snow water  
 192 equivalent of each REW was updated based on the snowfall (i.e., the solid precipitation) and  
 193 the snowmelt, and the snow cover area was then determined by the snow cover depletion curve  
 194 (Fassnacht et al., 2016). To simulate the evolution of glaciers, each REW is further divided into



195 several elevation bands to represent the change in temperature and precipitation along the  
196 altitudinal profile. The glacier within the intersection of each REW and elevation band is  
197 regarded as the representative unit for glacier simulation, similar to the discretization strategy  
198 adopted by Luo et al. (2013). For each glacier simulation unit, the model simulates the processes  
199 including the accumulation and melt of snow over glacier, the turnover of snow to ice, and the  
200 ice melt. More details and equations of the cryospheric module are provided in Nan et al. (2021b)  
201 and Cui et al. (2023).

202 The tracer module was incorporated into the model to simulate the isotope composition of  
203 multiple water bodies. The Rayleigh equation was adopted to simulate the isotope fractionation  
204 during water evaporation and snowmelt processes (He et al., 2019; Hindshaw et al., 2011). The  
205 isotope composition of glacier meltwater was assumed to be constantly more depleted than the  
206 local precipitation isotope and was estimated by an offset parameter (Nan et al., 2022). The  
207 isotope compositions in each simulation unit were calculated based on the complete mixing  
208 assumption. The isotope composition of snowpack and snowmelt was updated based on the  
209 water and isotope mass balance of the snowpack, similarly with other water storages. Forced  
210 by the precipitation isotope composition, the model can simulate the isotope composition of all  
211 water bodies, including stream water, soil water, groundwater, and snowpack. More details and  
212 calculation equations of the tracer module are provided in Nan et al. (2021b).

213 The THREW-T model quantified the contributions of multiple runoff components based  
214 on the flow-pathway definition as reviewed by He et al. (2021a). The runoff was firstly divided  
215 into surface runoff and subsurface runoff (baseflow) based on the runoff generation pathway.  
216 The surface runoff was then further divided into three components induced by different water  
217 sources (rainfall, snowmelt, and glacier melt). As a result, the total runoff was divided into four  
218 components: subsurface runoff, rainfall overland runoff, snowmelt overland runoff, and glacier  
219 melt overland runoff.

## 220 **2.4 Model calibration and evaluation**

221 The model was run for 25 years starting from 1991 to 2015, and was calibrated toward  
222 four objectives: the discharge at Nuxia station from 2001 to 2015, the snow cover area (SCA)  
223 from 2001 to 2015, the average glacier mass balance (GMB) from 2001 to 2010 in the whole

224 YTR basin, and the stream water isotope at the four stations in 2005. The Nash-Sutcliffe  
225 efficiency (NSE) was set as the evaluation metric for objectives with strong seasonality  
226 (discharge and isotope), and the root mean square error (RMSE) was set as the evaluation metric  
227 for objectives with essentially fluctuations (SCA and GMB) (Schaeffli and Gupta, 2007). The  
228 optimization objective function of calibration procedure was calculated by combining the  
229 function of each objective with equal weights.

230 An automatic algorithm, the Python Surrogate Optimization Toolbox (pySOT, Eriksson et  
231 al., 2019) were adopted for model calibration. The pySOT algorithm uses radial basis functions  
232 (RBFs) as surrogate models to approximate the simulations, reducing the time for each model  
233 run. The symmetric Latin hypercube design (SLHD) method was used to generate parameter  
234 values, allowing an arbitrary number of design points. In each optimization run, the procedure  
235 stopped when a maximum number of allowed function evaluations was reached, which was set  
236 as 3000. In this study, the pySOT algorithm was repeated for 100 times, and a final parameter  
237 set was selected from the calibrated parameter sets manually based on the overall performance  
238 on multiple objectives. The physical basis, reference ranges and calibrated values of the  
239 calibrated parameters in the THREW-T model are shown in Table 3.

240 Apart from the calibration functions, the model performances were additionally evaluated  
241 by four statistical metrics: logarithmic NSE (lnNSE), RMSE-observations standard deviation  
242 ratio (RSR), Percent bias (PBIAS) and correlation coefficient (CC). The discharge simulation  
243 was evaluated by lnNSE to examine the simulation of baseflow process. Our previous studies  
244 indicated that the discharge simulation performance during validation was highly correlated  
245 with that of calibration period, partly due to the strong linearity of precipitation-discharge  
246 relation in such a large basin, but large uncertainties existed in the discharge simulation at  
247 internal stations even when the discharge at outlet station was simulated well (Nan et al., 2021b,  
248 2022). Consequently, we not only conducted temporal validation based on the discharge data  
249 at Nuxia station during 1991~2000, but also collected additional discharge data at eight internal  
250 stations to assess the spatial consistency of model performance. The RMSE and CC of the  
251 cumulative glacier mass balance since the beginning of simulation period were also calculated  
252 to assess the glacier simulation, considering the temporal interpolation adopted by Hugonnet et  
253 al. (2021) which led to uncertainty in the year scale data.

254 
$$\text{NSE} = 1 - \frac{\sum(X_o - X_s)^2}{\sum(X_o - \bar{X}_o)^2} \quad (1)$$

255 
$$\ln\text{NSE} = 1 - \frac{\sum(\ln(X_o) - \ln(X_s))^2}{\sum(\ln(X_o) - \ln(\bar{X}_o))^2} \quad (2)$$

256 
$$\text{RMSE} = \sqrt{\frac{\sum(X_o - X_s)^2}{n}} \quad (3)$$

257 
$$\text{RSR} = \frac{\text{RMSE}}{\text{STD}_{\text{obs}}} = \frac{\sqrt{\sum(X_o - X_s)^2}}{\sqrt{\sum(X_o - \bar{X}_o)^2}} \quad (4)$$

258 
$$\text{PBIAS} = \frac{\sum(X_o - X_s) * 100}{\sum X_o} \quad (5)$$

259 
$$\text{CC} = \frac{\sum[(X_s - \bar{X}_s)(X_o - \bar{X}_o)]}{\sqrt{\sum[(X_s - \bar{X}_s)^2(X_o - \bar{X}_o)^2]}} \quad (6)$$

260 where,  $X_s$ ,  $X_o$ ,  $\bar{X}_s$  and  $\bar{X}_o$  are the simulated, observed, mean of simulated and mean of  
 261 observed hydrological variables, respectively, and  $n$  is the number of data.

262 **Table 3.** Physical descriptions, reference ranges and calibrated values of the calibrated  
 263 parameters in the THREW-T model

Symbol	Unit	Description	Reference range	Calibrated value
WM	cm	Tension water storage capacity used to calculate the saturation area	0~10	2.92
B	-	Shape coefficient used to calculate the saturation area	0~1	0.04
KKA	-	Exponential coefficient to calculate the subsurface runoff outflow rate	0~6	5.92
KKD	-	Linear coefficient to calculate the subsurface runoff outflow rate	0~0.5	0.21
DDF <sub>S</sub>	Mm/°C/d	Degree day factor for snowmelt	0~10	2.60
DDF <sub>G</sub>	Mm/°C/d	Degree day factor for glacier melt	0~10	1.51
T <sub>0</sub>	°C	Temperature threshold above which snow and glaciers melting occurs	-5 ~ 5	-4.28
C <sub>1</sub>	-	Coefficient to calculate concentration process using the Muskingum method	0~1	0.04
C <sub>2</sub>	-	Coefficient to calculate concentration process using the Muskingum method	0~1	0.80

264 **2.5 Perturbed climatic scenarios design**

265 Daily temperature and precipitation data extracted from the CMFD dataset were set as the  
 266 reference climate inputs. Linearly perturbed temperature and precipitation time series were  
 267 adopted to represent the potential climate change ranges. Perturbed temperature input data was  
 268 generated by adding one-degree increments to the reference daily temperature. The maximum

269 temperature increase was set as 5 °C, because the temperature in the YTR basin is projected to  
 270 increase at 1°C/20 yrs, and will increase by about 5 °C until the end of this decade (Cui et al.,  
 271 2023). The influence of changing temperature on the potential evapotranspiration was estimated  
 272 by the regression between the two factors (Eq. 7) which was developed by Van Pelt et al. (2009)  
 273 and widely adopted in the projection of potential evapotranspiration (e.g., Xu et al., 2019; Cui  
 274 et al., 2023).

$$275 \quad E_p = [1 - \alpha_0(T - \overline{T_0})] \cdot \overline{E_{p0}} \quad (7)$$

276 where,  $\overline{T_0}$  and  $\overline{E_{p0}}$  are the mean daily temperature and potential evapotranspiration in each  
 277 REW during the simulation period, respectively. T is the daily temperature generated by the  
 278 perturbation method.  $\alpha_0$  is determined by regressing the input daily potential  
 279 evapotranspiration and temperature in each REW.

280 Perturbed precipitation input data was generated by multiplying the reference daily  
 281 precipitation data from 80% to 120% with an increment of 10%, similar to Su et al. (2023)  
 282 which analyzed the runoff change of three basins on the TP under hypothesized climate change  
 283 scenarios. Simulation during 2001~2015 was set as the reference scenario, because the data of  
 284 most objectives/stations were available during this period. In total, one reference simulation,  
 285 five simulations of perturbed temperature and four simulations of perturbed precipitation were  
 286 conducted. To focus on the influence of climate perturbations on the hydrological processes,  
 287 the changes of underlying conditions such as soil and vegetation were not considered. In each  
 288 scenario, the standard deviations (STD) of the simulated annual hydrological variables were  
 289 calculated to represent the uncertainties introduced by natural climate variability. The t-Test  
 290 analysis of paired two samples was conducted for the annual hydrological variables produced  
 291 by reference scenario and each climate perturbation scenarios, to analyze the statistical  
 292 significance of the changes. Apart from the basic hydrological variables, the concentration ratio  
 293 (CR) and concentration period (CP) (Jiang et al., 2022a) were calculated by Eqs. 8~10 to  
 294 characterize the runoff seasonality.

$$295 \quad CR = \sqrt{R_x^2 + R_y^2} / \sum_{i=1}^{12} R_i \quad (8)$$

$$296 \quad CP = \arctan (R_x/R_y) \quad (9)$$

$$297 \quad R_x = \sum_{i=1}^{12} R_i \times \sin (\theta_i); R_y = \sum_{i=1}^{12} R_i \times \cos (\theta_i) \quad (10)$$

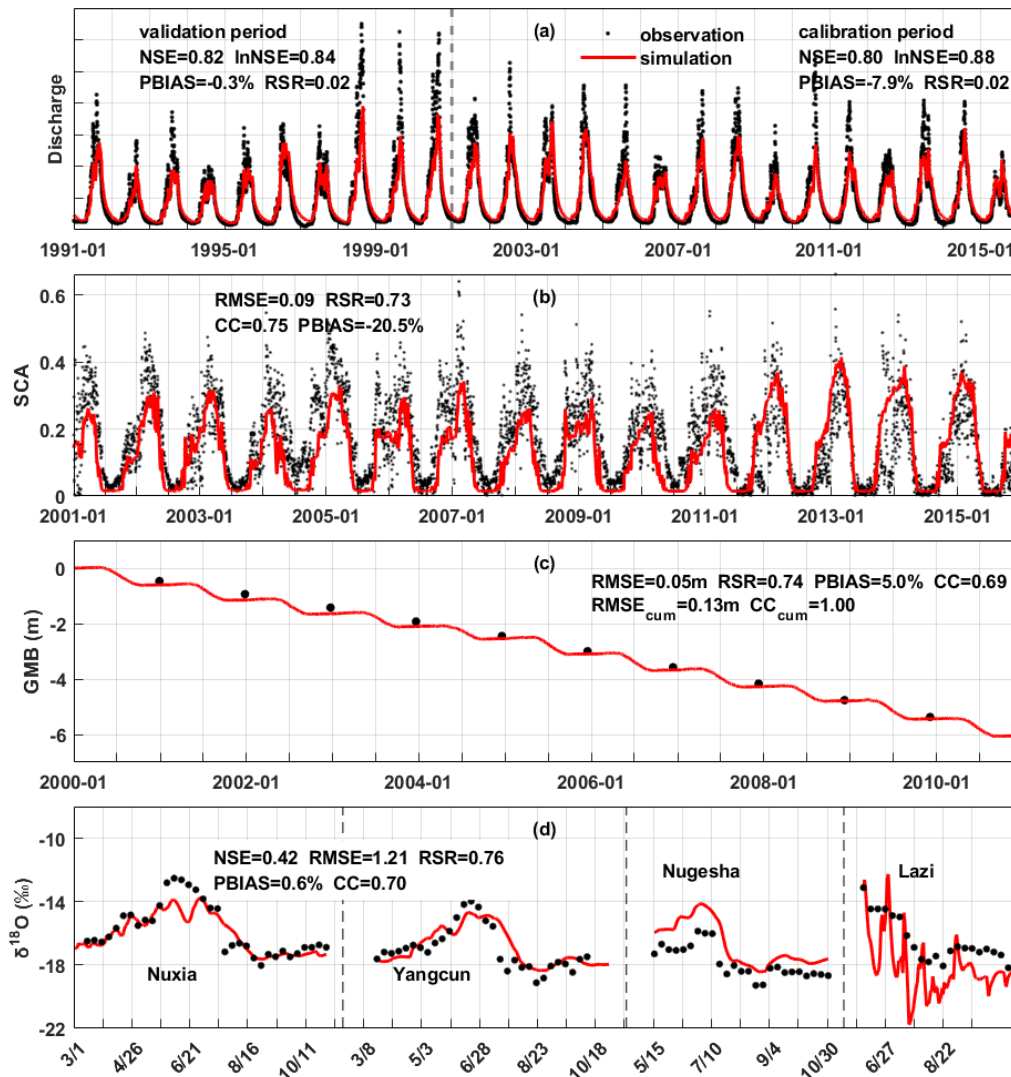
298 where,  $R_i$  is the runoff in the  $i$ th month,  $R_x$  and  $R_y$  are the resulting vectors in the direction of  $x$   
299 and  $y$ , respectively.  $\theta_i=360^\circ/12\times i=30^\circ\times i$  ( $i=1,2,\dots,12$ ).

### 300 **3. Results**

#### 301 **3.1 Model performance evaluation**

302 Figure 2 shows the model performances on the four calibration objectives. The discharge  
303 was simulated well regarding both high flow and baseflow processes, as indicated by the high  
304 NSE (0.82) and lnNSE (0.84). The occurring times of peak flow were captured by the model,  
305 showing the consistency in the temporal dynamics of simulated and observed streamflow, but  
306 the simulated magnitudes of peak flow were slightly lower than the observation (Figure 2a),  
307 partly due to the poor abilities of precipitation products on accurately capturing the high  
308 precipitation in high elevation elevations and the amount of specific precipitation extreme  
309 events (Li et al., 2021; Jiang et al., 2022b; Xu et al., 2017). The performance of discharge  
310 simulation during validation period was similar with that of calibration period, with NSE and  
311 lnNSE of 0.80 and 0.88 respectively, as shown in Figure 2a. Nonetheless, the simulated annual  
312 runoff (302 mm/yr) was very close to the observation (303 mm/yr), indicating that the amount  
313 of total runoff was reproduced well. The simulated variation of SCA was smoother than the  
314 observation, but the seasonality was captured well, i.e., decreasing sharply in May and  
315 remaining extremely low from July to September (Figure 2b). The low RMSE ( $<0.1$ ) suggested  
316 that the model performed well on simulating the snow processes. The model successfully  
317 simulated the declining glacier (Figure 2c), with an extremely high CC for the cumulative  
318 glacier mass balance ( $\sim 1$ ). The model estimated the annual GMB in the YTR basin as -0.545  
319 m/yr, very close to the value extracted from the dataset of Hugonnet et al. (2021) (-0.554 m/yr).  
320 The calibrated melting temperature threshold was rather low ( $-4.28^\circ\text{C}$ ), which was partly due  
321 to the fact that melting processes were simulated at the daily step. The model simulated the  
322 variation of stream isotope well, indicated by the high NSE, CC and low PBIAS, which  
323 provided confidence in the partitioning among different runoff components (Nan et al., 2021a;  
324 He et al., 2019). The seasonality of the isotope was adequately captured: getting enriched in  
325 May, reaching maximum in June, and getting depleted in late June/early July (Figure 2d). The  
326 fact that the model simultaneously satisfied four calibration objectives ensured the proper

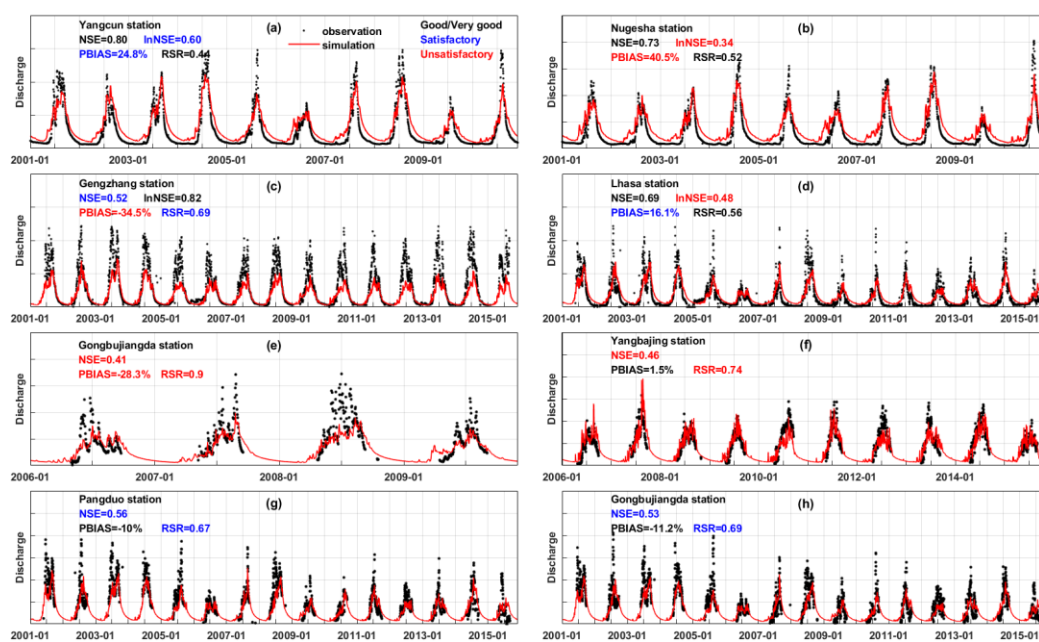
327 representation of the hydrological and cryospheric processes, and provided a reasonable  
 328 baseline for the sensitivity analysis.



329  
 330 **Figure 2.** The model performances on the calibration objectives. (a) the streamflow discharge  
 331 at Nuxia station, (b) the snow cover area ratio in the YTR basin, (c) the average glacier mass  
 332 balance in the YTR basin, and (d) the stream water isotope at four stations in 2005.

333 Figure 3 shows the streamflow simulation at eight internal stations. The performance  
 334 ratings were evaluated based on four metrics following the guideline by Moriasi et al. (2007).  
 335 At the two stations located along the mainstream (Yangcun and Nugesha), the high flow  
 336 processes were simulated well as indicated by the high NSE, but the baseflows were  
 337 overestimated (Figure 3a and b). In contrast, the high flow processes were underestimated at  
 338 Gengzhang station, but the baseflows were reproduced well (Figure 3c). The model produced  
 339 fair performance on both high flow and baseflow simulation at Lhasa station, showing moderate

340 NSE and lnNSE (Figure 3d). For the four stations where only the data during the wet season  
 341 were available, the PBIASs were at good levels (within  $\pm 15\%$ ) except for Gongbujiangda  
 342 station (Figure 3e-h). Overall, the streamflow simulations at internal stations were not as good  
 343 as the calibrated outlet station, but were at acceptable levels, as indicated by at least one  
 344 satisfactory metric except for Gongbujiangda station. The high flow processes and runoff  
 345 amount were reproduced relatively well, as indicated by the generally satisfactory NSE and  
 346 PBIAS. But the small time-scale fluctuations and extremes were mostly not captured well,  
 347 because the model was not evaluated toward metrics related to hydrological signatures  
 348 (McMillan et al., 2017; Majone et al., 2022; Fenicia et al., 2018). Nonetheless, the validation  
 349 based on the internal stations gave confidence in the spatial pattern of the hydrological  
 350 processes and their sensitivities to the perturbed climate.



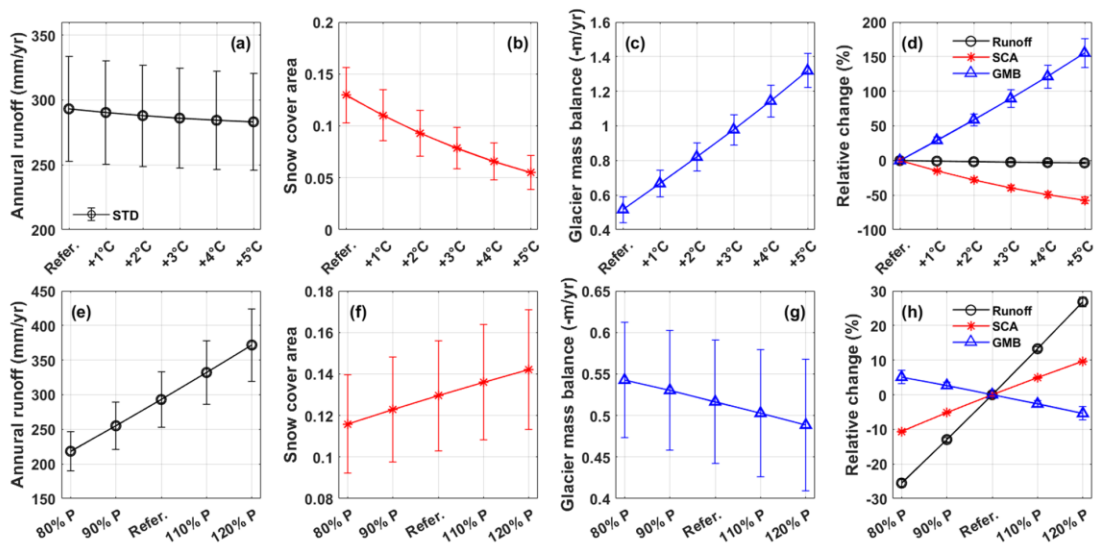
351

352 **Figure 3.** The model performances on the streamflow simulation at the internal stations.

### 353 3.2 Sensitivities of hydrological variables to perturbed temperature and precipitation

354 The sensitivities of annual runoff, snow cover area, and glacier mass balance to perturbed  
 355 temperature and precipitation are shown in Figure 4. The relationships between hydrological  
 356 variables and precipitation/temperature showed strong linearity, which was similar with Su et  
 357 al. (2023) analyzing the hydrological sensitivities in three other large basins on the TP ( $\sim 10^5$   
 358  $\text{km}^2$ ), but was different from He et al. (2021b) which conducted a similar analysis in a small  
 359 boreal forest basin in Canada ( $603 \text{ km}^2$ ). The annual runoff kept decreasing significantly with

360 the increasing temperature at the rate of  $-2 \text{ mm}/^\circ\text{C}$  due to the increasing evaporation (Figure  
 361 4a). The decreasing rate got small when the temperature increase was higher than  $3^\circ\text{C}$ , partly  
 362 because the controlling factor of evaporation changed from energy limitation to water limitation  
 363 (Wang et al., 2022). The runoff change in response to increasing temperature was rather small  
 364 compared to the intra-annual runoff variability. The snow cover area ratio significantly reduced  
 365 with the increasing temperature at the rate of  $-1.5\%/^\circ\text{C}$  because of the decreasing snowfall and  
 366 increasing snowmelt, and would be smaller than half of the reference scenario for  $5^\circ\text{C}$  of  
 367 warming (Figure 4b). The glacier mass balance significantly got more negative with the  
 368 increasing temperature because of the reducing accumulation and increasing meltwater, at the  
 369 rate of  $-0.16 \text{ m}/^\circ\text{C}$  (Figure 4c). Among the three variables, the glacier mass balance was the  
 370 most sensitive to the warming climate, the relative change of which could be 150% for  $5^\circ\text{C}$  of  
 371 warming (Figure 4d). The changes of runoff, snow cover area and glacier mass balance in  
 372 response to increasing temperature were all statistically significant at 0.01 significance level.



373  
 374 **Figure 4.** The sensitivities of annual runoff, snow cover area, and glacier mass balance to the  
 375 perturbed temperature (a-d) and precipitation (e-g). Subplots (d) and (h) are the relative changes  
 376 of runoff, SCA and GMB compared to the reference scenario.

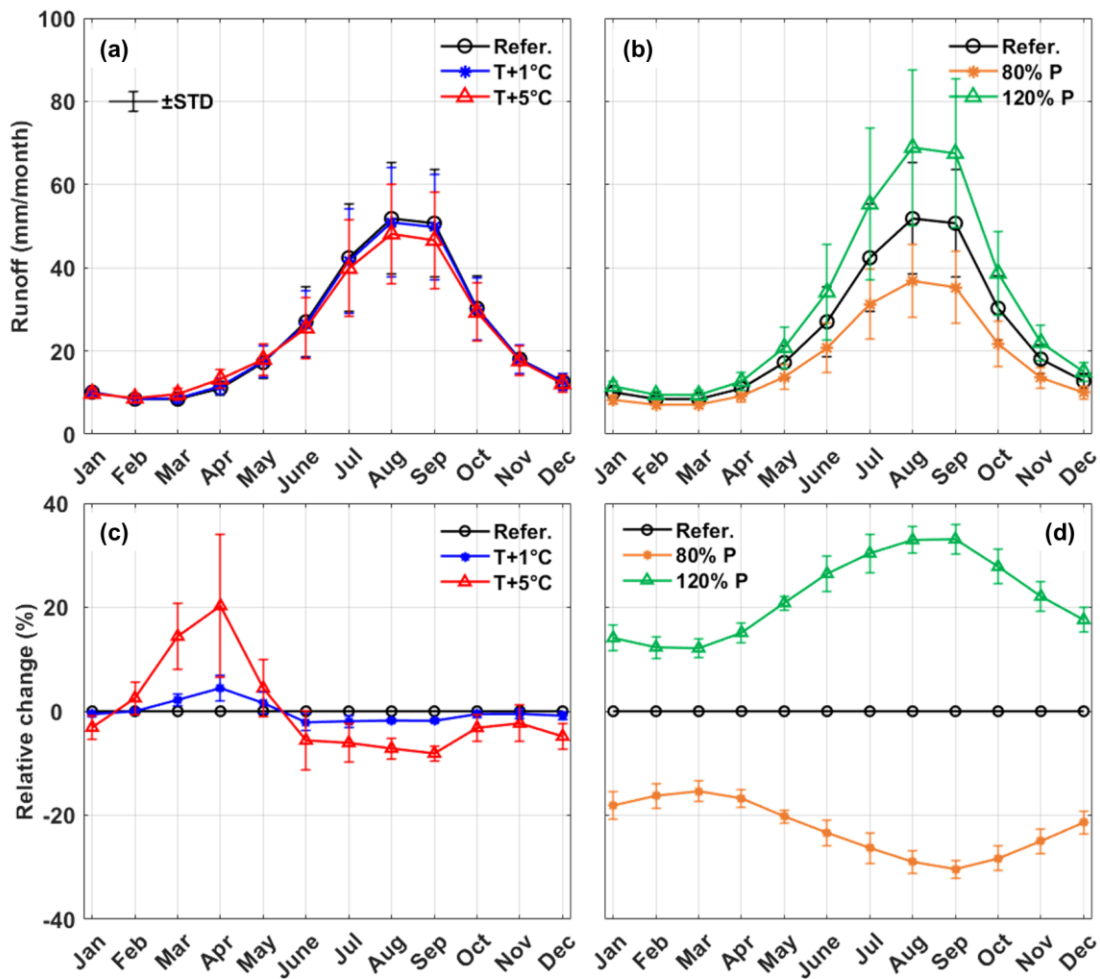
377 The hydrological sensitivities to perturbed precipitation were opposite to that of  
 378 temperature. The annual runoff increased at the rate of  $38.4 \text{ mm}/10\%$  with the increasing  
 379 precipitation (Figure 4e). The relative change in runoff was larger than precipitation (Figure  
 380 4h), indicating an increasing runoff coefficient with increasing precipitation. This also indicated



381 a small relative change in evaporation in response to precipitation perturbation, again  
382 suggesting that the energy limitation played more important role than water limitation on  
383 evaporation in the reference scenario. With the increasing precipitation, the snow cover area  
384 increased at 0.7%/10%, and the glacier mass balance got more positive at 0.014m/10% because  
385 of the larger amount of snowfall and snow/ice accumulation (Figure 4f and 4g). Among the  
386 three variables, the runoff had the highest sensitivity to perturbed precipitation, with a relative  
387 change rate of 13%/10% (Figure 4h), while the changes of snow cover area and glacier mass  
388 balance were within the range of  $\pm 10\%$  when precipitation changed by 20%. The changes of  
389 runoff, snow cover area and glacier mass balance in response to perturbed precipitation were  
390 all statistically significant at 0.01 significance level.

### 391 **3.3 Sensitivities of runoff variation to perturbed temperature and precipitation**

392 The sensitivities of inter- and intra-annual runoff variation to perturbed temperature and  
393 precipitation are shown in Figure 5. The average monthly runoff were calculated based on the  
394 simulated hydrographs during the entire simulation period, and the inter-annual runoff variation  
395 was represented by the STD. The change of inter-annual runoff variation was consistent with  
396 that of total runoff. The inter-annual runoff variations were also lower in the scenarios with less  
397 runoff (increasing temperature or decreasing precipitation), showing the narrower ranges of the  
398 error bars in Figure 5a-b, and vice versa. Despite the decreasing runoff caused by increasing  
399 temperature, the average runoff for 5°C of warming was still much higher than the lower error  
400 bar of the reference scenario (Figure 5a), suggesting that the runoff change tendency caused by  
401 the increasing temperature was relatively small compared to the inherent runoff variability. On  
402 the contrary, when precipitation increased by 20%, the average annual runoff was higher than  
403 the runoff in wet years of reference scenario (Figure 5b), indicating that the trend of  
404 precipitation change had a larger influence on the runoff than the inter-annual variation of  
405 precipitation.



406  
 407 **Figure 5.** Sensitivities of intra- and inter-annual streamflow variability to the perturbed  
 408 temperature and precipitation. (a) and (b) monthly runoff, (c) and (d) relative change of monthly  
 409 runoff.

410 The sensitivities of monthly runoff were different among months. Although increasing  
 411 temperature led to a decrease in the total runoff, it caused an increasing spring runoff. The  
 412 monthly runoff in April increased most significantly, which increased 20% for 5°C of warming  
 413 (Figure 5e). This could be attributed to the increasing snowmelt, because the SCA decreased  
 414 significantly during the same period (Figure 2b). The monthly runoff in all twelve months  
 415 changed accordingly to perturbed precipitation, but the change during wet seasons (August to  
 416 October) was the most significant (Figure 5f). The different monthly runoff sensitivities in  
 417 response to perturbed temperature and precipitation indicated that temperature changes  
 418 influenced more on baseflow, while precipitation changes had higher impact on high flow  
 419 processes. As a result, increasing temperature caused a more even distribution of monthly

runoff, while increasing precipitation had the opposite effect. The CR decreased from 0.432±0.044 to 0.402±0.046 for the warming of 5°C, indicating a more even seasonal runoff distribution caused by increasing temperature. The CP decreased by around two days, indicating that climate warming would result in advance of maximum runoff. The STD of CP slightly increased from 7.09 days at the reference scenario to 7.45 days for the warming of 5°C. On the contrary, the CR changed from 0.398±0.039 to 0.465±0.045 when precipitation increased from 80% to 120% of the reference, indicating that increasing precipitation made the distribution of runoff more concentrated. The CP advanced by 2.2 days in response to a 20% decreasing precipitation, but only recessed by 0.3 days in response to an increasing precipitation with the same magnitude. Similar with the response to warming temperature, the STD of CP also slightly increased in response to increasing precipitation. The change of CR was significant at significance level of 0.01 in all scenarios, but the change of CP was insignificant in some scenarios, including T +1°C, 110% P and 120% P, with p value of 0.014, 0.02 and 0.12, respectively.

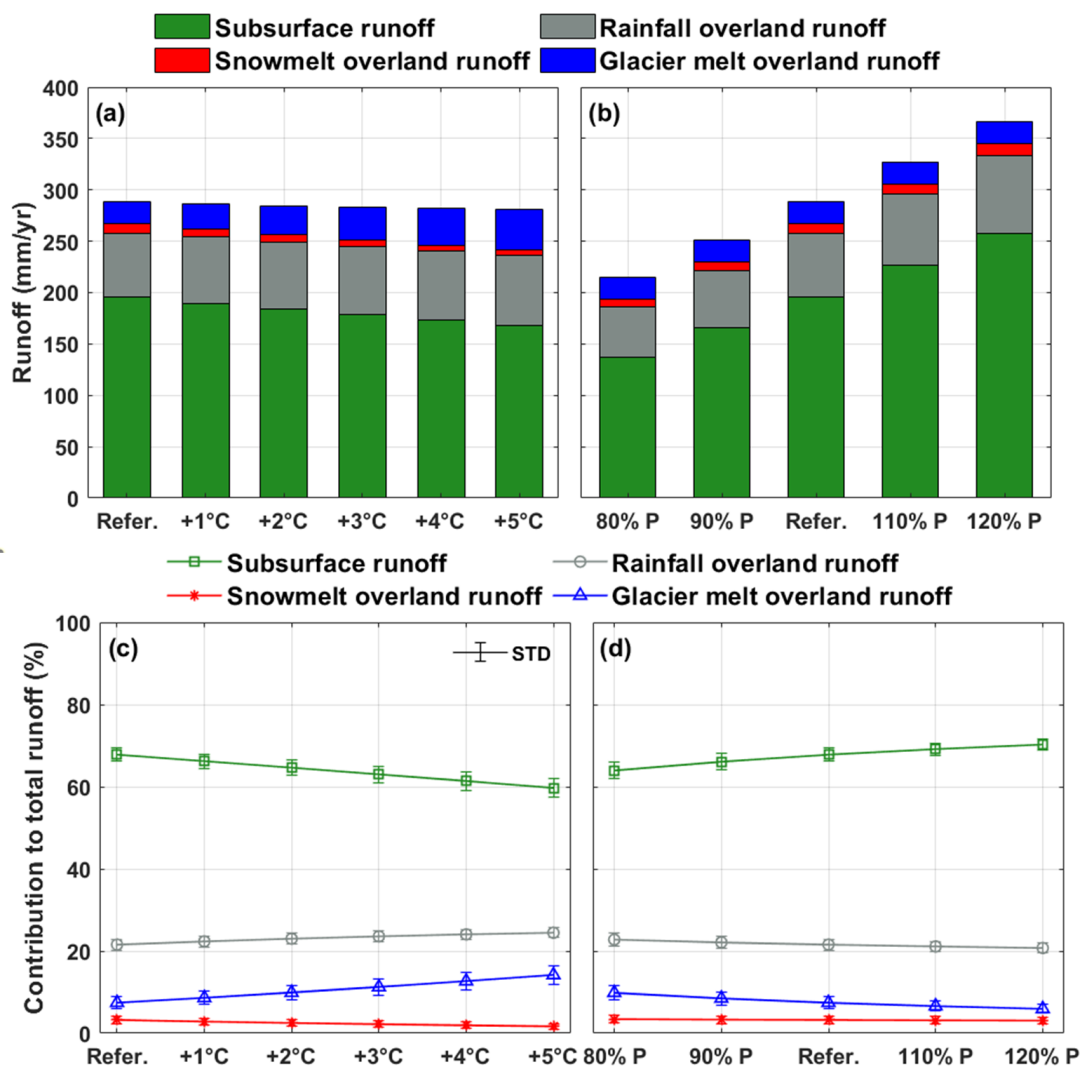
**Table 4.** The concentration ratio (CR) and concentration period (CP) of runoff in different scenarios with perturbed temperature and precipitation

		CR		CP (days)	
		Average	STD	Average	STD
Reference scenario		0.432	0.044	244.4	7.09
T scenario	+1°C	0.425	0.044	244.1	7.12
	+2°C	0.419	0.045	243.8	7.18
	+3°C	0.413	0.045	243.3	7.26
	+4°C	0.408	0.046	242.8	7.36
	+5°C	0.402	0.046	242.3	7.45
P scenario	80%	0.398	0.039	242.2	6.86
	90%	0.415	0.042	243.6	7.01
	110%	0.449	0.045	244.7	7.13
	120%	0.465	0.045	244.7	7.14

### 3.4 Sensitivities of runoff components to perturbed temperature and precipitation

The contributions of runoff components in the YTR basin under scenarios with different temperature and precipitation are shown in Figure 6. In the reference scenario, the subsurface runoff was the dominant component, contributing 67.8±1.7% to the total runoff. Among the three surface runoff components, rainfall was the dominant water source contributing 21.6±1.3%

441 to the total runoff. Glacier melt overland runoff had considerable contribution to the runoff  
 442 which contributed  $7.4 \pm 1.4\%$  to the total runoff, while the contribution of snowmelt overland  
 443 runoff was only  $3.2 \pm 0.9\%$ . The annual subsurface runoff was  $195.8 \pm 31.0$  mm/yr ( $39.2 \pm 6.2$   
 444  $\text{km}^3/\text{yr}$ ), close to the amount ( $30 \text{ km}^3/\text{yr}$ ) estimated by Yao et al. (2021) with the groundwater  
 445 model MODFLOW. It should be noted that in our model all the glacier meltwater was assumed  
 446 to generate surface runoff directly because of the impermeable glacier surface, while the  
 447 snowmelt was assumed to be partitioned into two components (infiltration and surface runoff)  
 448 (Nan et al., 2021b, 2023; Schaeffli et al., 2005).



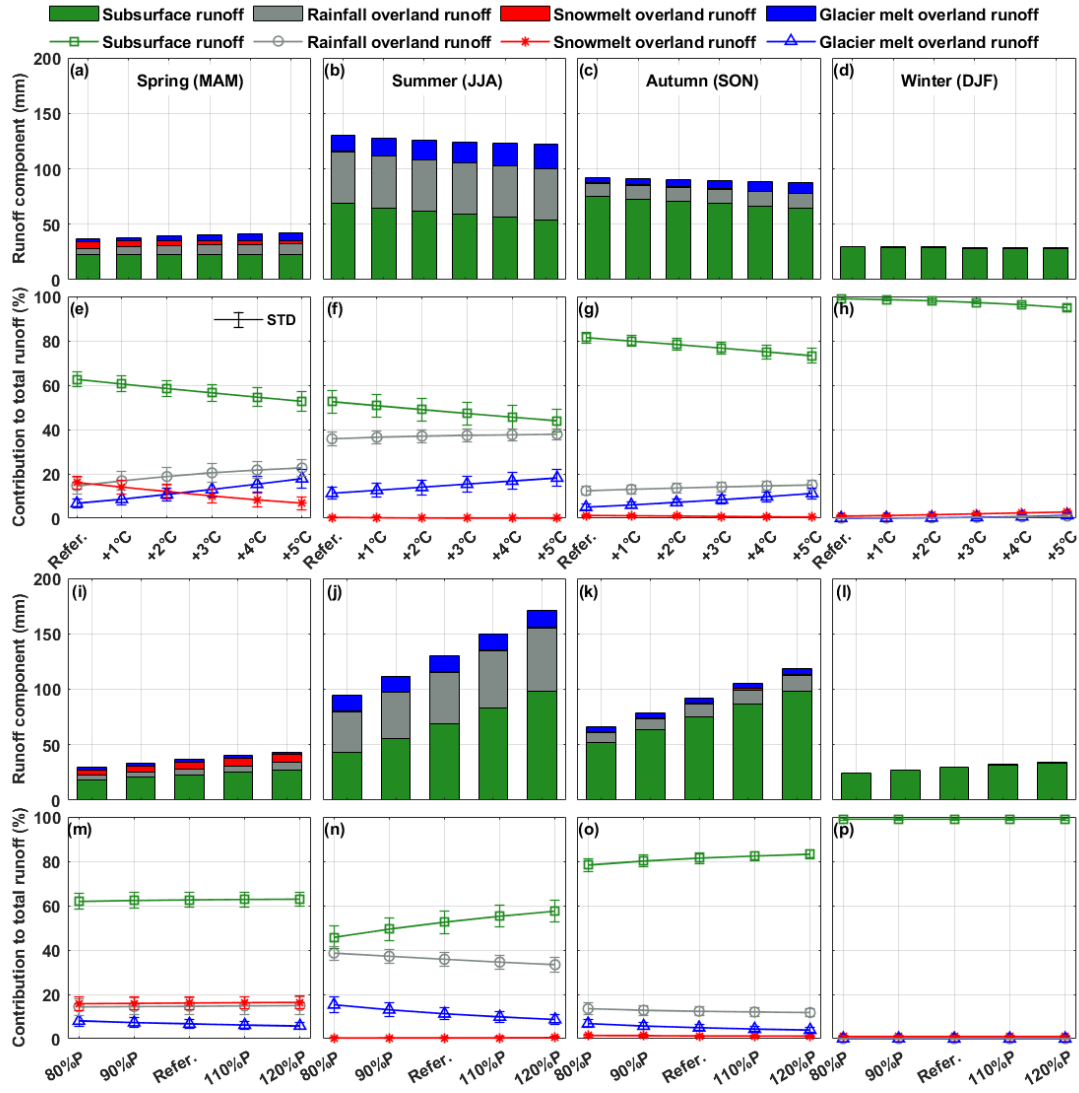
449  
 450 **Figure 6.** Sensitivities of the runoff components to perturbed temperature and precipitation.  
 451 (a) and (b) amounts of runoff components, (c) and (d) contributions of runoff components to  
 452 the total runoff.

453 With the increasing temperature, the amount and proportion of subsurface runoff decreased

454 at  $-5.6\text{mm}/^{\circ}\text{C}$  and  $-1.6\%/^{\circ}\text{C}$ , because climate warming increased evaporation and consequently  
455 reduced the subsurface water storage and outflow. The rainfall and snowmelt overland runoff  
456 increased at  $1.3\text{mm}/^{\circ}\text{C}$  ( $0.6\%/^{\circ}\text{C}$ ) and decreased at  $-0.9\text{mm}/^{\circ}\text{C}$  ( $-0.3\%/^{\circ}\text{C}$ ), respectively,  
457 because more rainfall was partitioned from total precipitation due to higher temperature. The  
458 glacier melt overland runoff increased significantly at  $3.7\text{mm}/^{\circ}\text{C}$  ( $1.4\%/^{\circ}\text{C}$ ) with the increasing  
459 temperature, and the contribution to total runoff could be around 15% for  $5^{\circ}\text{C}$  of warming. The  
460 amount of all four runoff components increased with the increasing precipitation (Figure 6b),  
461 with rates of  $30.1\text{mm}/10\%$ ,  $6.8\text{mm}/10\%$ ,  $1.0\text{mm}/10\%$  and  $0.1\text{mm}/10\%$  for subsurface, rainfall  
462 overland, snowmelt overland and glacier melt overland runoff, respectively. However, only the  
463 proportion of subsurface runoff increased at  $1.6\%/10\%$  with the increasing precipitation, while  
464 the proportions of three other components all decreased, with rates of  $-0.5\%/10\%$ ,  $-0.1\%/10\%$   
465 and  $-1.0\%/10\%$  for rainfall overland, snowmelt overland and glacier melt overland runoff,  
466 respectively (Figure 6d), because there was a much higher increase in the total runoff. Overall,  
467 the contributions of runoff components were more sensitive to temperature perturbation than  
468 precipitation perturbation.

469 Figure 7 and Tables S1-S4 show the runoff components in different seasons and their  
470 sensitivities to perturbed climate. The subsurface runoff was the dominant component in all  
471 four seasons in the reference scenario, with contribution ranging from 53% in summer to 99%  
472 in winter. The contribution of snowmelt overland runoff was extremely low in the seasons  
473 except for spring because of the small SCA in summer and autumn and the low temperature in  
474 winter. The contribution of snowmelt overland runoff in spring was close to that of rainfall  
475 overland runoff (Figure 7e-h). The contribution of glacier melt overland runoff was around half  
476 that of rainfall overland runoff in all four seasons. With climate warming, the contribution of  
477 subsurface runoff decreased in all four seasons, while the contributions of rainfall and glacier  
478 melt overland runoff increased. The significantly increasing glacier melt and rainfall led to an  
479 increase in the total runoff in spring (Figure 7a). The contribution of snowmelt overland runoff  
480 decreased in three seasons except for winter, during which its contribution slightly increased,  
481 and got around 3% for  $5^{\circ}\text{C}$  of warming (Figure 7h). With increasing precipitation, the amounts  
482 of four components increased in all seasons (Figure 7i-l), but the contributions of components  
483 remained nearly unchanged in spring, autumn and winter (Figure 7m, o-p). The contributions

484 of runoff components were sensitive to perturbed precipitation only in summer, during which  
 485 subsurface runoff contributed more to the runoff with increasing precipitation, while the  
 486 contributions of rainfall and glacier melt overland runoff decreased significantly (Figure 7n).



487  
 488 **Figure 7.** Sensitivities of the seasonal runoff components to perturbed temperature and  
 489 precipitation. (a)-(d) sensitivities of amounts of runoff components to perturbed temperature,  
 490 (e)-(h) sensitivities of contributions of runoff components to perturbed temperature, (i)-(l)  
 491 sensitivities of amounts of runoff components to perturbed precipitation, (m)-(p) sensitivities  
 492 of contributions of runoff components to perturbed precipitation.

### 493 3.5 Spatial pattern of local hydrological sensitivities

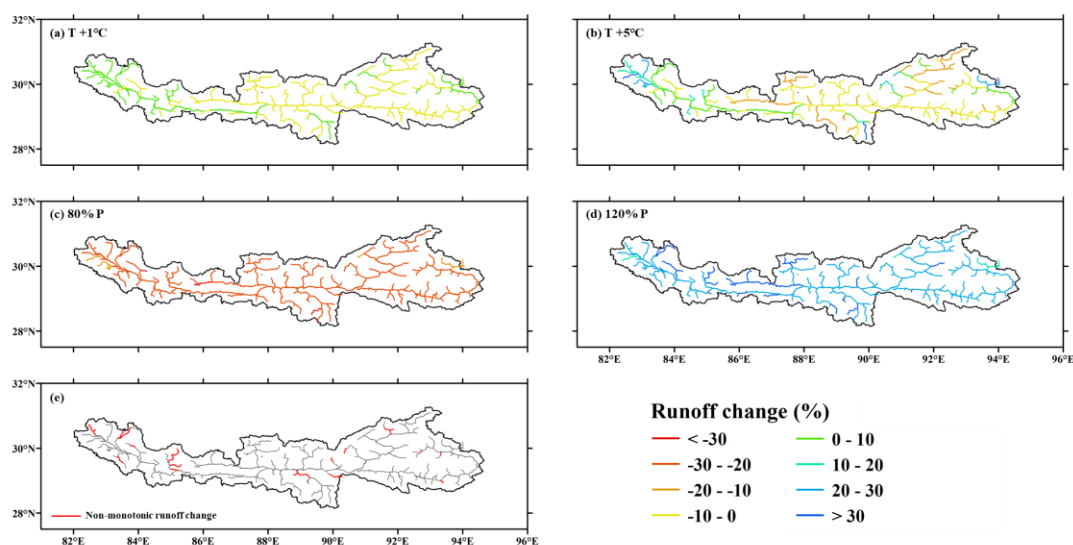
494 Considering that the YTR basin is a large basin with drainage area of  $2 \times 10^5 \text{ km}^2$ , the spatial  
 495 pattern of the local hydrological sensitivity was further analyzed with the assistance of the

496 spatially distributed model structure. The runoff change at REW scale in four typical scenarios  
497 (i.e., 1°C of warming, 5°C of warming, precipitation changing to 80% and 120%) are shown in  
498 Figure 8. All REWs have the same runoff trend with the precipitation perturbation (Figure 8c  
499 and 8d). The runoff increasing ranged from 12.2% to 40.4% when precipitation increased by  
500 20%. In most REWs, the runoff changed at larger rates than precipitation, with few exceptions  
501 located in the tributaries of Nyang River, Lhasa River and the source region of mainstream,  
502 showing shallow red/blue colors in Figure 8c and 8d. On the contrary, the REW scale runoff  
503 changes in response to increasing temperature had strong spatial variability (Figure 8a and 8b).  
504 Although the runoff at the basin outlet decreased with climate warming, the REW scale runoff  
505 increased in about half of REWs. For 5°C of warming, the REW scale runoff changes ranged  
506 from -18.6% to 54.3%. Most REWs with increasing runoff were located upstream of the  
507 mainstream, the Nianchu River, the Nyang River, and the tributary of Lhasa River (Figure 8b).

508 The statistical significance of runoff change in response to climate perturbation was  
509 analyzed. The runoff change in response to perturbed precipitation was significant in all the  
510 REWs, but things were different for warming temperature scenarios. The number of REWs  
511 with insignificant change trend decreased with the temperature warming level. In specify, the  
512 runoff change was insignificant (at significance level of 0.01) in 26% and 15% area of the whole  
513 basin, for the warming of 1°C and 5°C, respectively (Figure S1). The statistical significance in  
514 response to warming temperature was related to the runoff change magnitude and drainage area  
515 (Figure S2). Consequently, although the runoff change at basin outlet was rather small  
516 (decreasing by 0.9% and 3.4% for the warming of 1°C and 5°C, respectively), it was still  
517 statistically significant.

518 The runoff in some REWs changed non-monotonically with increasing temperature, i.e.,  
519 the runoff change trend was reversed in different temperature intervals. Most of such non-  
520 monotonic REWs were located in the upstream region of the mainstream, with some others  
521 located in the major tributaries Nyang River, Lhasa River and Nianchu River (Figure 8e). In  
522 about 75% of non-monotonic REWs, the runoff first decreased for 1°C of warming, and then  
523 changed to an increasing trend at higher warming levels, and the reserved trends occurred in  
524 the other 25% of REWs. The threshold temperature of trend turning differed among non-  
525 monotonic REWs, which was 3°C in about half of the REWs. The runoff change rates in

526 response to increasing temperature were generally low in non-monotonic REWs, most within  
 527 the range of  $\pm 1\%/^{\circ}\text{C}$ .



528  
 529 **Figure 8.** The change of REW scale runoff in response to perturbed temperature and  
 530 precipitation. (a) and (b) runoff change in response to temperature perturbation, (c) and (d)  
 531 runoff change in response to precipitation perturbation, (e) the locations of REWs showing non-  
 532 monotonic runoff change in response to increasing temperature.

## 533 4. Discussions

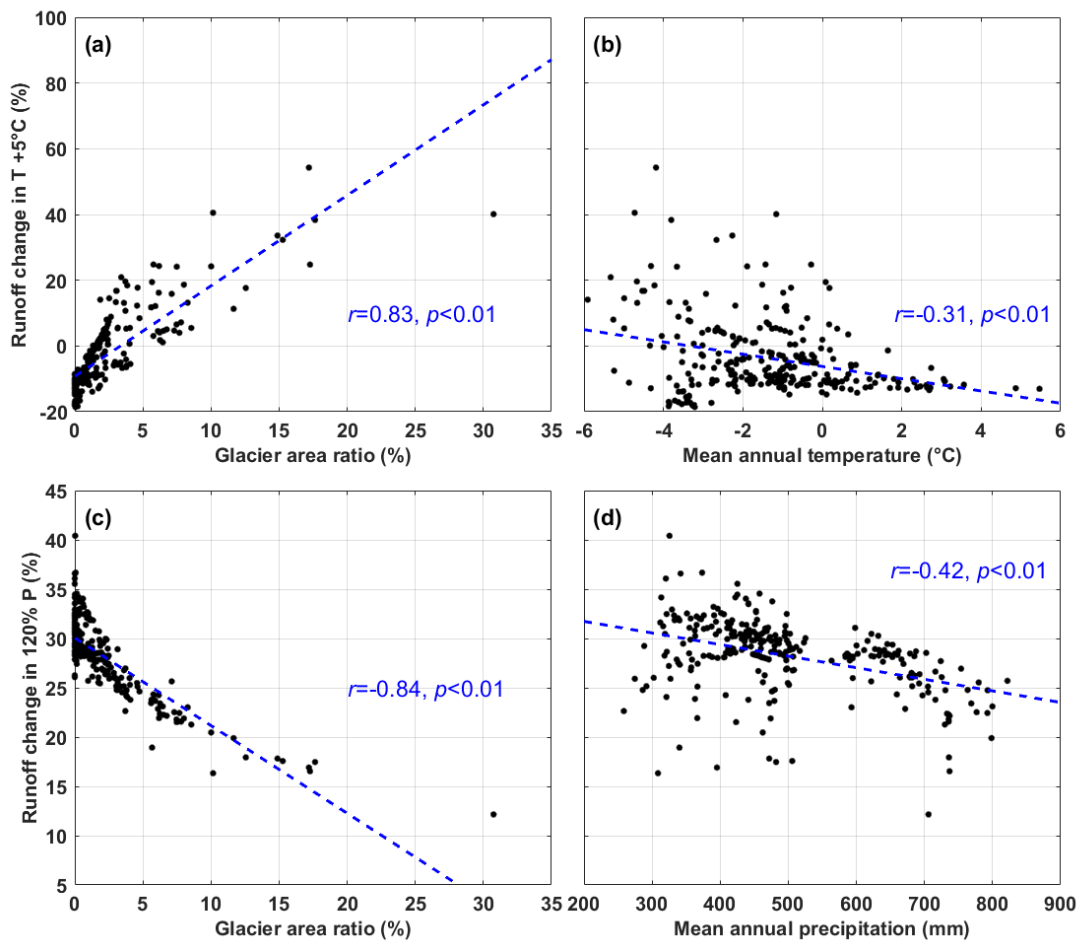
### 534 4.1 The influence factors of local hydrological sensitivities: the role of glaciers

535 Our results show the strong spatial variability of the REW scale hydrological sensitivities  
 536 to perturbed climate. Consequently, the influence factors of the local sensitivities are analyzed  
 537 in this section. The basic characteristics, including mean annual temperature (MAT), mean  
 538 annual precipitation (MAP), average elevation (ELE), drainage area (DRA), and glacier area  
 539 ratio (GAR) were calculated for each REW as the potential factors. It should be noted that,  
 540 considering the runoff concentration processes between the upstream and downstream REWs,  
 541 the above characteristics were not calculated solely within each REW, but for the total drainage  
 542 area controlled by each REW. The correlations between the runoff change for  
 543 temperature/precipitation increasing by  $5^{\circ}\text{C}/20\%$  and the potential influence factors were  
 544 analyzed. The relations with the two factors with the highest coefficients are shown in Figure  
 545 9. Detailed data and relations with lower coefficients are shown in Table S5 and Figure S3.

546 The GAR was the most correlated factor for the hydrological sensitivities to the



547 perturbation of both temperature and precipitation, with coefficients higher than 0.8 (Figure 9a  
548 and 9c). The runoff change for 5°C of warming increased with the increasing GAR (Figure 9a),  
549 because of the balance between the decreasing runoff caused by evaporation and the increasing  
550 runoff contributed by glacier melt. In REWs where the GAR was higher than a threshold, the  
551 increasing glacier melt could offset the increasing evaporation, and the runoff increased with  
552 climate warming. The threshold GAR was different among REWs, ranging from 1~5%. For the  
553 REWs with GAR larger than 10%, the runoff increase for 5°C of warming could be higher than  
554 20%. The hydrological sensitivity to increasing temperature also had a weak but significant  
555 negative correlation ( $r=-0.31$ ,  $p<0.01$ ) with the MAT of the REW (Figure 9b), which could be  
556 partly attributed to the interrelation between GAR and MAT, i.e., the GAR tended to be lower  
557 in warmer regions, and the runoff consequently decreased in response to increasing temperature.  
558 A lower bound of runoff change could be observed in Figure 9b for the REWs with relatively  
559 high MAT, again indicating the different limitation factors of evaporation, i.e., in relatively  
560 warm regions, the evaporation was limited by the water condition, so increasing temperature  
561 did not cause more evaporation (Wang et al., 2022).



562

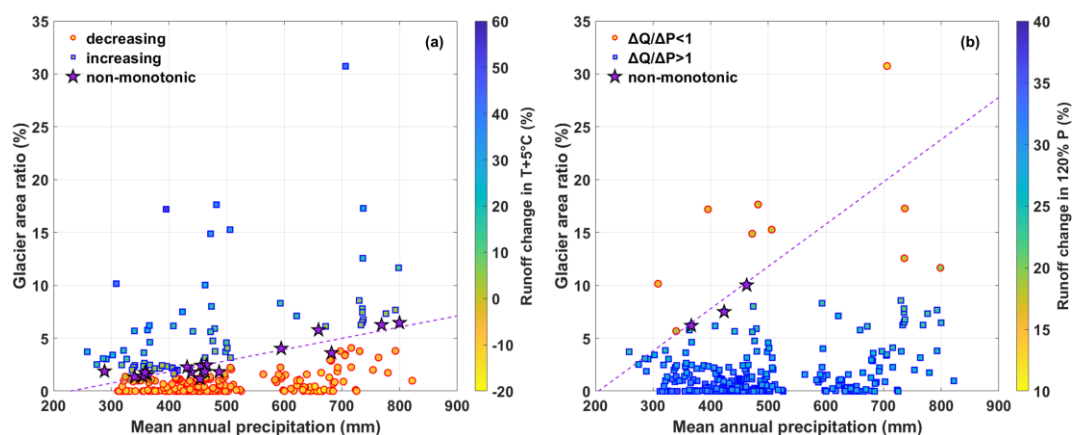
563 **Figure 9.** The correlations between the hydrological sensitivities to climate perturbation and  
 564 the dominant influence factors.

565 On the contrary, the runoff change in response to increasing precipitation had a significant  
 566 negative correlation ( $r=-0.84, p<0.01$ ) with the GAR (Figure 9c), mainly due to the spatial  
 567 variability of the runoff components. In REWs with larger GAR, the contribution of  
 568 precipitation-induced runoff was relatively low due to the large contribution of glacier melt  
 569 runoff, thus the influence of increasing precipitation on runoff change was also small. It should  
 570 be noted that based on regression line in Figure 9c, the runoff change would be around zero in  
 571 regions with GAR higher than 35, which was a rather surprising inference. This might be due  
 572 to the small sample of REWs with high GAR based on current spatial discretization, resulting  
 573 in the poor confidence in the end of the regression line. The runoff change in response to  
 574 increasing temperature also negatively correlated with the MAP ( $r=-0.42, p<0.01$ , Figure 9d).  
 575 The contribution of subsurface runoff component was higher in wetter conditions (Figure 6d),  
 576 resulting in more evaporation and a lower runoff coefficient, which caused a relatively small

577 increase in runoff, similar with the finding by He et al. (2021b).

578 Our results indicate that the runoff in some REWs changed non-monotonically in response  
579 to the increasing temperature. The characteristics of these non-monotonic REWs were further  
580 analyzed. Interestingly, the GAR of non-monotonic REWs had a good linear relationship with  
581 their MAP (Figure 10a). The regression equation of the linear relation was  
582  $GAR(\%)=0.011*MAP(mm)-2.43$  ( $r=0.92$ ). Moreover, this regression line was the dividing line  
583 between the REWs where runoff increased with increasing temperature and those with opposite  
584 runoff trends in the GAR-MAP plot (Figure 10a). The REWs located in the upper part of the  
585 plot had larger runoff increasing rates. This indicated that the local hydrological sensitivity to  
586 increasing temperature was determined by the relationship between GAR and MAP. In wetter  
587 REWs with larger MAP, more glaciers were needed to offset the decreasing runoff due to the  
588 increasing temperature and evaporation. These findings suggested the important role of glaciers  
589 in determining the runoff change in response to climate change. Similar characteristics were  
590 observed in the precipitation perturbation scenarios (Figure 10b). The runoff change rate was  
591 different from the precipitation change rate in all REWs, and was consistently either higher or  
592 lower than precipitation change rate in most REWs. But there were three REWs shifting from  
593  $\Delta Q/\Delta P < 1$  to  $> 1$ , the GAR and MAP of which also had linear relationship, forming the boundary  
594 of REWs where runoff changed more significantly than precipitation and those with lower  
595 runoff change rate. However, there were only three such non-monotonic REWs for precipitation  
596 perturbation scenarios, providing less confidence to the boundary line. As a result, there were  
597 some REWs lying lower than the boundary line but with lower runoff change rate than  
598 precipitation (Figure 10b).

599



600 **Figure 10.** The interrelation among the REW scale glacier area ratio, mean annual  
601 precipitation and the runoff change for (a) 5°C of warming and (b) 120% precipitation.

#### 602 **4.2 Implications of the sensitivity analysis**

603 The sensitivity analysis indicated the important role of glaciers in providing meltwater to  
604 offset the runoff decreasing caused by climate warming. Our study showed that glacier  
605 meltwater had a limited contribution to the total runoff in the YTR basin, similar with some  
606 recent studies (Wang et al., 2021; Cui et al., 2023), resulting in a decreasing runoff trend with  
607 increasing temperature. However, the spatial pattern analysis indicated that the role of glacier  
608 melt runoff could be rather significant in the regions with large area covered by glaciers. For  
609 example, the runoff increased significantly in the Yangbajing tributary of the Lhasa River in  
610 response to increasing temperature (Figure 8), consistent with previous research estimating a  
611 high contribution of glacier melt to runoff in this region (Lin et al., 2020; Wang et al., 2023). It  
612 is therefore necessary to address the spatial scale issue when discussing the role of glacier  
613 meltwater on water resources.

614 Several studies have stressed the important role of glaciers on the TP as the largest global  
615 store of frozen water which supplied freshwater resources to downstream regions (Yao et al.,  
616 2022). This study quantitatively estimated the role of glacier meltwater in offsetting the  
617 decreasing runoff with increasing temperature and evaporation. Our results indicated that the  
618 influences of glacier on hydrological processes were highly dependent on the spatial scale and  
619 the local meteorological characteristics. Specifically, the role of glacier meltwater would  
620 undoubtedly be more significant in regions with larger glacier cover areas (Luo et al., 2018;  
621 Zhao et al., 2019; Khanal et al., 2021). Meanwhile, the role of glaciers was smaller in wetter  
622 regions with higher precipitation because of the relatively low contribution of glacier meltwater  
623 in total runoff. Consequently, the regions with larger precipitation amounts but little glacier  
624 coverage would face a greater risk of water resources shortage in a warming future (Figure 10a),  
625 and other regions would face the similar condition because of the shrinking glacier area. Our  
626 results also suggested a larger influence of precipitation change on runoff than that of  
627 temperature change (Figure 4), thus an accurate projection of precipitation is crucial for the  
628 assessment of water resources under climate change. Recent studies showed a decreasing

629 precipitation trend after 2000 in the YTR basin (Li et al., 2016; Luan and Zhai, 2022), likely  
630 posing threats of water scarcity to the riparian regions and again highlighting the important role  
631 of glacier in maintaining water resources.

632 Our results showed that the runoff responded to increasing temperature non-monotonically  
633 in some regions. These non-monotonic REWs represented the most dynamic regions within the  
634 basin, as they kept shifting between energy and water limited stages. Recent studies also  
635 projected the non-monotonic runoff change on the TP at increasing warming levels (Cui et al.,  
636 2023), i.e., the annual mean runoff for major rivers on the TP will significantly decrease by  
637 0.1~3.2% at the warming level of 1.5°C, and increase by 1.5~12% at 3.0°C in the future.  
638 Although seemingly similar, the two studies revealed two different phenomena. In particular,  
639 the non-monotonic runoff change projected by Cui et al. (2023) was driven by the output put  
640 of climatic projection data CMIP6 (Eyring et al., 2016), and the runoff change was dominated  
641 by the tendencies and periodicities of climate factors, especially precipitation (Wu et al., 2022).  
642 Our study analyzed the runoff change in response to climate warming with fixed precipitation  
643 input, and the trend was the result of the comprehensive response of multiple water balance  
644 components to climate change. The local non-monotonic hydrological sensitivity was  
645 essentially a borderline condition of increasing and decreasing trend, which reflected the  
646 balance of increasing meltwater and evaporation in response to climate warming.

647

### 648 **4.3 Limitations**

649 This study explored the sensitivities of hydrological processes to climate change by  
650 designing temperature and precipitation perturbation scenarios, rather than projecting future  
651 runoff using the forcing data from general circulation models (GCMs). The assumed climate  
652 perturbation method is widely used in runoff projection studies (He et al., 2021b; Su et al., 2023;  
653 Rasouli et al., 2014; Rasouli et al., 2015), with the advantage of avoiding the computation cost  
654 of correcting biases and downscaling GCMs to regional scale (Piani et al., 2010; Xu et al.,  
655 2019). However, the assumed climate perturbation did not reflect the gradual process of climate  
656 change. Specifically, the temperature should go through relatively low warming levels before  
657 arriving at the assumed highest level, but the climate perturbation method actually assumed an

658 abrupt climate change. Because of the relatively short simulation period, the potential trend  
659 turning of meltwater caused by the combined effect of increasing melting rate and shrinking  
660 glacier area cannot be reflected by the sensitivity analysis (Yao et al., 2022; Zhang et al., 2022a).  
661 We can expect that the role of glaciers when temperature increases by 5°C in the future should  
662 be less than our results, because the glacier covered area at that time will be less than the current  
663 condition (Yao et al., 2022). Meanwhile, the potential influences of temperature and  
664 precipitation change on soil and vegetation conditions (Boulanger et al., 2016) were not  
665 considered when designing the climate perturbation scenarios. Besides, because climate  
666 perturbation rather than climate ensemble was used to force the model, the representation of  
667 uncertainties related to climate forcing was very simplified. Nonetheless, the simple sensitivity  
668 analysis in this study helped better understand the separate effect of changing temperature and  
669 precipitation on runoff, and informed the role of glaciers in controlling the spatial pattern of  
670 runoff change.

671 Another limitation comes from the uncertainties of hydrological model. Although  
672 validated by the measurement data of multiple objectives and several internal stations, the  
673 model still had potential uncertainties. First, as the most important forcing data, the common  
674 precipitation datasets in the YTR basin all had large uncertainties, due to the lack of validation  
675 data in high elevation regions (Xu et al., 2017), leading to uncertainties in hydrological  
676 simulation. The model underestimated the peak streamflow for most stations, which could be  
677 attributed to the underestimated precipitation during wet seasons by CMFD dataset. Further  
678 correction on the precipitation product based on more station data could be helpful to remove  
679 the bias. Second, because of the complex hydrological processes and runoff components, the  
680 parameter equifinality problem usually existed in the hydrological model in large mountainous  
681 basins (Gupta et al., 2008; Nan et al., 2021a). He et al. (2019) indicated that the uncertainties  
682 of runoff component contributions could be nearly 20% even when the simulations of  
683 streamflow, snow, glacier and isotope were satisfied simultaneously. The misestimation of the  
684 runoff regime would undoubtedly influence the sensitivity analysis. Third, the calibration  
685 procedure of this work was rather simple, based on a combination of automatic algorithm and  
686 manual selection. The influences of calibration scheme, optimized objective function (Gupta et  
687 al., 2009; Majone et al., 2022) and the weights of multiple objectives (Tong et al., 2021) on

688 hydrological sensitivities were not analyzed deeply. For instance, different types of evaluation  
689 metrics for multiple objectives were added together directly, which may result in different  
690 impacts on the integrated objective function. Besides, the use of pySOT algorithm did not allow  
691 for a comprehensive hydrological uncertainty analysis, because it aimed to achieve the best  
692 fitness between observations and model outputs. Lastly, the calibrated parameters were  
693 assumed to be spatially uniform within the whole basin to avoid introducing too many  
694 parameters. Although this is similar to several large-scale modeling studies (e.g., Cui et al.,  
695 2023; Lutz et al., 2014), the uniform parameter might be inadequate to represent the spatial  
696 variability of hydrological processes, which may influence some conclusions of the sensitivity  
697 analysis. For example, considering the potential spatial variability of glacier melting rate, the  
698 characteristics of non-monotonic REWs in Figure 10 may not form a straight line. Currently  
699 this work only considered the uncertainties introduced by natural climate variabilities. More  
700 works are needed in the future to analyze the parameter sensitivities and the uncertainties from  
701 calibration schemes.

## 702 **5. Conclusions**

703 This study adopted the tracer-aided hydrological model THREW-T in a typical large  
704 mountainous basin Yarlung Tsangpo River (YTR) on the Tibetan Plateau (TP). The model was  
705 validated against multiple objectives (streamflow, snow, glacier and isotope) and the  
706 streamflow at internal stations. The sensitivities of hydrological processes to perturbed  
707 temperature and precipitation were analyzed. The spatial pattern of local hydrological  
708 sensitivities and the influence factors were explored. Our main findings are as follows:

709 (1) The THREW-T model performed well on simulating the streamflow, snow cover area  
710 (SCA), glacier mass balance (GMB), and stream water isotope, ensuring good representation  
711 of the key cryospheric processes and a reasonable estimation of the contributions of runoff  
712 components. The model performed acceptably on simulating the streamflow at eight internal  
713 stations located in the mainstream and two major tributaries, which indicated that the spatial  
714 pattern of hydrological processes was reflected by the model, and provided confidence in the  
715 sensitivity analysis.

716 (2) Most hydrological characteristics responded to increasing temperature and

717 precipitation oppositely. Increasing temperature led to decreasing annual runoff, SCA and GMB,  
718 and changed the runoff variation showing a smaller inter-annual variation, a more even  
719 distributed intra-annual distribution, and an earlier maximum runoff. It also influenced the  
720 runoff regime by increasing the contributions of rainfall and glacier melt overland runoff, but  
721 decreasing the subsurface runoff and snowmelt overland runoff. Increasing precipitation had  
722 the opposite effects to increasing temperature.

723 (3) The distribution of local hydrological sensitivities had a strong spatial variability. The  
724 local runoff change in response to increasing temperature varied significantly, with changing  
725 rate of -18.6% to 54.3% for 5°C of warming. The glacier area ratio (GAR) was the dominant  
726 factor of the spatial pattern of hydrological sensitivities to both perturbed temperature and  
727 precipitation. Some regions had a non-monotonic runoff change rate in response to climate  
728 perturbation, which represented the most dynamic regions within the basin, as they kept shifting  
729 between energy and water limited stages. The GAR and mean annual precipitation (MAP) of  
730 the non-monotonic regions had a linear relation, and formed the boundary of regions with  
731 different runoff trends in the GAR-MAP plot.

732

### 733 **Code and data availability**

734 Code and data availability. The isotope data and the code of THREW-T model used in this study  
735 are available from the corresponding author (tianfq@tsinghua.edu.cn). Other data sets are  
736 publicly available as follows: DEM (<http://www.gscloud.cn/sources/details/310?pid=302>, last  
737 access: 1 January 2019, Geospatial Data Cloud Site, 2019), CMFD  
738 (<https://doi.org/10.11888/AtmosphericPhysics.tpe.249369.file>, Yang and He, 2019), glacier  
739 inventory data (<https://doi.org/10.3972/glacier.001.2013.db>, Liu, 2012), glacier elevation  
740 change data (<https://doi.org/10.6096/13>, Huggonet et al., 2021), NDVI  
741 (<https://doi.org/10.5067/MODIS/MOD13A3.006>, Didan, 2015), LAI  
742 (<https://doi.org/10.5067/MODIS/MOD15A2H.006>, Myneni et al., 2015), HWSD  
743 (<https://data.tpdc.ac.cn/zh-hans/data/3519536a-d1e7-4ba1-8481-6a0b56637baf/?q=HWSD>,  
744 last access: 1 January 2019, He, 2019). These datasets not publicly available are referred to in  
745 the main text (Chen et al., 2018; Liu et al., 2007).



746

747 **Author contribution**

748 YN conceived the idea and collected data; YN and FT conducted analysis and wrote the paper.

749

750 **Financial support**

751 This study has been supported by the National Natural Science Foundation of China (grant no.

752 92047301) and the Shuimu Tsinghua Scholar Program.

753

754 **Competing interests**

755 At least one of the (co-)authors is a member of the editorial board of Hydrology and Earth

756 System Sciences.

757

758 **References**

759 Aygun, O., Kinnard, C., Campeau, S., and Krogh, S. A.: Shifting Hydrological Processes in a

760 Canadian Agroforested Catchment due to a Warmer and Wetter Climate, *Water*, 12,

761 10.3390/w12030739, 2020.

762 Bai, X. L., Zhao, W. Z., Liu, H., Zhang, Y. Y., Yang, Q. Y., Liu, J. T., and Chang, X. L.: Effects

763 of precipitation changes and land-use alteration on streamflow: A comparative analysis

764 from two adjacent catchments in the Qilian Mountains, arid northwestern China, *Frontiers*

765 in Environmental Science, 11, 10.3389/fenvs.2023.1097049, 2023.

766 Birkel, C. and Soulsby, C.: Advancing tracer-aided rainfall-runoff modelling: a review of

767 progress, problems and unrealised potential, *Hydrological Processes*, 29, 5227-5240,

768 10.1002/hyp.10594, 2015.

769 Blöschl, G. and Montanari, A.: Climate change impacts-throwing the dice?, *Hydrological*

770 *Processes*, 24, 374-381, 10.1002/hyp.7574, 2010.

771 Boulanger, Y., Taylor, A. R., Price, D. T., Cyr, D., McGarrigle, E., Rammer, W., Sainte-Marie,

772 G., Beaudoin, A., Guindon, L., and Mansuy, N.: Climate change impacts on forest

773 landscapes along the Canadian southern boreal forest transition zone, *Landscape Ecology*,

774 32, 1415-1431, 10.1007/s10980-016-0421-7, 2017.

775 Cao, L. G. and Pan, S. M.: Changes in precipitation extremes over the "Three-River  
776 Headwaters" region, hinterland of the Tibetan Plateau, during 1960-2012, *Quaternary  
777 International*, 321, 105-115, 10.1016/j.quaint.2013.12.041, 2014.

778 Chen, X., Long, D., Liang, S., He, L., Zeng, C., Hao, X., and Hong, Y.: Developing a composite  
779 daily snow cover extent record over the Tibetan Plateau from 1981 to 2016 using  
780 multisource data, *Remote Sensing of Environment*, 215, 284-299,  
781 10.1016/j.rse.2018.06.021, 2018.

782 Criss, R. E. and Winston, W. E.: Do Nash values have value? Discussion and alternate proposals,  
783 *Hydrological Processes*, 22, 2723-2725, 10.1002/hyp.7072, 2008.

784 Cui, T., Li, Y., Yang, L., Nan, Y., Li, K., Tudaji, M., Hu, H., Long, D., Shahid, M., Mubeen, A.,  
785 He, Z., Yong, B., Lu, H., Li, C., Ni, G., Hu, C., and Tian, F.: Non-monotonic changes in  
786 Asian Water Towers' streamflow at increasing warming levels, *Nature communications*,  
787 14, 1176-1176, 10.1038/s41467-023-36804-6, 2023.

788 Didan, K.: MOD13A3 MODIS/Terra vegetation Indices Monthly L3 Global 1 km SIN Grid  
789 V006, NASA EOSDIS Land Processes DAAC [dataset],  
790 <https://doi.org/10.5067/MODIS/MOD13A3.006>, 2015.

791 Eriksson, D., Bindel, D., and Shoemaker, C. A.: pySOT and POAP: An event-driven  
792 asynchronous framework for surrogate optimization, *arXiv preprint*,  
793 10.48550/arXiv.1908.00420, 2019.

794 Eyring, V., Bony, S., Meehl, G. A., Senior, C. A., Stevens, B., Stouffer, R. J., and Taylor, K. E.:  
795 Overview of the Coupled Model Intercomparison Project Phase 6 (CMIP6) experimental  
796 design and organization, *Geoscientific Model Development*, 9, 1937-1958, 10.5194/gmd-  
797 9-1937-2016, 2016.

798 Fassnacht, S. R., Sexstone, G. A., Kashipazha, A. H., Ignacio Lopez-Moreno, J., Jasinski, M.  
799 F., Kampf, S. K., and Von Thaden, B. C.: Deriving snow-cover depletion curves for  
800 different spatial scales from remote sensing and snow telemetry data, *Hydrological  
801 Processes*, 30, 1708-1717, 10.1002/hyp.10730, 2016.

802 Fenicia, F., Kavetski, D., Reichert, P., and Albert, C.: Signature-Domain Calibration of  
803 Hydrological Models Using Approximate Bayesian Computation: Empirical Analysis of

804 Fundamental Properties, *Water Resources Research*, 54, 3958-3987,  
805 10.1002/2017wr021616, 2018.

806 Gao, J., Yao, T. D., Masson-Delmotte, V., Steen-Larsen, H. C., and Wang, W. C.: Collapsing  
807 glaciers threaten Asia's water supplies, *Nature*, 565, 19-21, 10.1038/d41586-018-07838-4,  
808 2019.

809 Gupta, H. V., Kling, H., Yilmaz, K. K., and Martinez, G. F.: Decomposition of the mean squared  
810 error and NSE performance criteria: Implications for improving hydrological modelling,  
811 *Journal of Hydrology*, 377, 80-91, 10.1016/j.jhydrol.2009.08.003, 2009.

812 Gupta, H. V., Wagener, T., and Liu, Y.: Reconciling theory with observations: elements of a  
813 diagnostic approach to model evaluation, *Hydrological Processes*, 22, 3802-3813,  
814 10.1002/hyp.6989, 2008.

815 He, Y.: Pan-TPE soil map based on Harmonized World Soil Database (V1.2), National Tibetan  
816 Plateau Data Center [dataset], 2019.

817 He, Z. H. and Pomeroy, J. W.: Assessing hydrological sensitivity to future climate change over  
818 the Canadian southern boreal forest, *Journal of Hydrology*, 624,  
819 10.1016/j.jhydrol.2023.129897, 2023.

820 He, Z., Duethmann, D., and Tian, F.: A meta-analysis based review of quantifying the  
821 contributions of runoff components to streamflow in glacierized basins, *Journal of*  
822 *Hydrology*, 603, 10.1016/j.jhydrol.2021.126890, 2021a.

823 He, Z. H., Pomeroy, J. W., Fang, X., and Peterson, A.: Sensitivity analysis of hydrological  
824 processes to perturbed climate in a southern boreal forest basin, *Journal of Hydrology*, 601,  
825 10.1016/j.jhydrol.2021.126706, 2021b.

826 He, Z., Unger-Shayesteh, K., Vorogushyn, S., Weise, S. M., Kalashnikova, O., Gafurov, A.,  
827 Duethmann, D., Barandun, M., and Merz, B.: Constraining hydrological model parameters  
828 using water isotopic compositions in a glacierized basin, Central Asia, *Journal of*  
829 *Hydrology*, 571, 332-348, 10.1016/j.jhydrol.2019.01.048, 2019.

830 Hindshaw, R. S., Tipper, E. T., Reynolds, B. C., Lemarchand, E., Wiederhold, J. G., Magnusson,  
831 J., Bernasconi, S. M., Kretzschmar, R., and Bourdon, B.: Hydrological control of stream  
832 water chemistry in a glacial catchment (Damma Glacier, Switzerland), *Chemical Geology*,  
833 285, 215-230, 10.1016/j.chemgeo.2011.04.012, 2011.

834 Hugonnet, R., McNabb, R., Berthier, E., Menounos, B., Nuth, C., Girod, L., Farinotti, D., Huss,  
835 M., Dussailant, I., Brun, F., and Kaab, A.: Accelerated global glacier mass loss in the early  
836 twenty-first century, *Nature*, 592, 726-+, 10.1038/s41586-021-03436-z, 2021.

837 Immerzeel, W. W., van Beek, L. P. H., and Bierkens, M. F. P.: Climate Change Will Affect the  
838 Asian Water Towers, *Science*, 328, 1382-1385, 10.1126/science.1183188, 2010.

839 Jiang, Y., Xu, Z., and Xiong, L.: Runoff variation and response to precipitation on multi-spatial  
840 and temporal scales in the southern Tibetan Plateau, *Journal of Hydrology-Regional  
841 Studies*, 42, 10.1016/j.ejrh.2022.101157, 2022a.

842 Jiang, Y., Yang, K., Yang, H., Lu, H., Chen, Y., Zhou, X., Sun, J., Yang, Y., and Wang, Y.:  
843 Characterizing basin-scale precipitation gradients in the Third Pole region using a high-  
844 resolution atmospheric simulation-based dataset, *Hydrology and Earth System Sciences*,  
845 26, 4587-4601, 10.5194/hess-26-4587-2022, 2022b.

846 Khanal, S., Lutz, A. F., Kraaijenbrink, P. D. A., van den Hurk, B., Yao, T., and Immerzeel, W.  
847 W.: Variable 21st Century Climate Change Response for Rivers in High Mountain Asia at  
848 Seasonal to Decadal Time Scales, *Water Resources Research*, 57, 10.1029/2020wr029266,  
849 2021.

850 Li, X., Yao, Z., Xiao, J., and Wang, H.: Analysis of the spatial-temporal variation characteristics  
851 of precipitation over the Tibetan Plateau from 1961 through 2010, *Journal of Glaciology  
852 and Geocryology*, 38, 1233-1240, 2016.

853 Li, C., Sinha, E., Horton, D. E., Diffenbaugh, N. S., and Michalak, A. M.: Joint bias correction  
854 of temperature and precipitation in climate model simulations, *Journal of Geophysical  
855 Research-Atmospheres*, 119, 13153-13162, 10.1002/2014jd022514, 2014.

856 Li, Z. X., Feng, Q., Li, Z. J., Yuan, R. F., Gui, J., and Lv, Y. M.: Climate background, fact and  
857 hydrological effect of multiphase water transformation in cold regions of the Western  
858 China: A review, *Earth-Science Reviews*, 190, 33-57, 10.1016/j.earscirev.2018.12.004,  
859 2019.

860 Li, Z. J., Li, Z. X., Song, L. L., Gui, J., Xue, J., Zhang, B. J., and Gao, W. D.: Hydrological and  
861 runoff formation processes based on isotope tracing during ablation period in the source  
862 regions of Yangtze River, *Hydrology and Earth System Sciences*, 24, 4169-4187,  
863 10.5194/hess-24-4169-2020, 2020.

864 Li, K., Tian, F., Khan, M. Y. A., Xu, R., He, Z., Yang, L., Lu, H., and Ma, Y.: A high-accuracy  
865 rainfall dataset by merging multiple satellites and dense gauges over the southern Tibetan  
866 Plateau for 2014-2019 warm seasons, *Earth System Science Data*, 13, 5455-5467,  
867 10.5194/essd-13-5455-2021, 2021.

868 Lin, L., Gao, M., Liu, J., Wang, J., Wang, S., Chen, X., and Liu, H.: Understanding the effects  
869 of climate warming on streamflow and active groundwater storage in an alpine catchment:  
870 the upper Lhasa River, *Hydrology and Earth System Sciences*, 24, 1145-1157,  
871 10.5194/hess-24-1145-2020, 2020.

872 Liu, S.: The second glacier inventory dataset of China (version 1.0) (2006–2011), National  
873 Tibetan Plateau Data Center [dataset], 10.3972/glacier.001.2013.db, 2012.

874 Liu, Z. F., Tian, L. D., Yao, T. D., Gong, T. L., Yin, C. L., and Yu, W. S.: Temporal and spatial  
875 variations of delta O-18 in precipitation of the Yarlung Zangbo River Basin, *Journal of*  
876 *Geographical Sciences*, 17, 317-326, 10.1007/s11442-007-0317-1, 2007.

877 Luan, L. and Zhai, P.: Changes in rainy season precipitation properties over the Qinghai-Tibet  
878 Plateau based on multi-source datasets, *Progressus Inquisitiones de Mutatione Climatis*,  
879 19, 173-190, 2023.

880 Luo, Y., Arnold, J., Liu, S., Wang, X., and Chen, X.: Inclusion of glacier processes for  
881 distributed hydrological modeling at basin scale with application to a watershed in  
882 Tianshan Mountains, northwest China, *Journal of Hydrology*, 477, 72-85,  
883 10.1016/j.jhydrol.2012.11.005, 2013.

884 Luo, Y., Arnold, J., Liu, S. Y., Wang, X. Y., and Chen, X.: Inclusion of glacier processes for  
885 distributed hydrological modeling at basin scale with application to a watershed in  
886 Tianshan Mountains, northwest China, *Journal of Hydrology*, 477, 72-85,  
887 10.1016/j.jhydrol.2012.11.005, 2013.

888 Luo, Y., Wang, X., Piao, S., Sun, L., Ciais, P., Zhang, Y., Ma, C., Gan, R., and He, C.:  
889 Contrasting streamflow regimes induced by melting glaciers across the Tien Shan - Pamir  
890 - North Karakoram, *Scientific Reports*, 8, 10.1038/s41598-018-34829-2, 2018.

891 Luo, Y., Wang, X. L., Piao, S. L., Sun, L., Ciais, P., Zhang, Y. Q., Ma, C. K., Gan, R., and He,  
892 C. S.: Contrasting streamflow regimes induced by melting glaciers across the Tien Shan -  
893 Pamir - North Karakoram, *Scientific Reports*, 8, 10.1038/s41598-018-34829-2, 2018.

894 Lutz, A. F., Immerzeel, W. W., Shrestha, A. B., and Bierkens, M. F. P.: Consistent increase in  
895 High Asia's runoff due to increasing glacier melt and precipitation, *Nature Climate Change*,  
896 4, 587-592, 10.1038/nclimate2237, 2014.

897 Majone, B., Avesani, D., Zulian, P., Fiori, A., and Bellin, A.: Analysis of high streamflow  
898 extremes in climate change studies: how do we calibrate hydrological models?, *Hydrology  
899 and Earth System Sciences*, 26, 3863-3883, 10.5194/hess-26-3863-2022, 2022.

900 McMillan, H., Westerberg, I., and Branger, F.: Five guidelines for selecting hydrological  
901 signatures, *Hydrological Processes*, 31, 4757-4761, 10.1002/hyp.11300, 2017.

902 Moriasi, D. N., Arnold, J. G., Van Liew, M. W., Bingner, R. L., Harmel, R. D., and Veith, T. L.:  
903 Model evaluation guidelines for systematic quantification of accuracy in watershed  
904 simulations, *Transactions of the Asabe*, 50, 885-900, 10.13031/2013.23153, 2007.

905 Myneni, R., Knyazikhin, Y., and Park, T.: MOD15A2H MODIS/Terra Leaf Area Index/FPAR  
906 8-Day L4 Global 500 m SIN Grid V006, NASA EOSDIS Land Processes DAAC [dataset],  
907 10.5067/MODIS/MOD15A2H.006, 2015.

908 Nan, Y., Tian, F., Li, Z., and Gui, J.: Longer simulation time step of the tracer-aided hydrological  
909 model estimates lower contribution of slow runoff components, *Journal of Hydrology*,  
910 <https://doi.org/10.1016/j.jhydrol.2023.129889>, 2023.

911 Nan, Y., He, Z., Tian, F., Wei, Z., and Tian, L.: Can we use precipitation isotope outputs of  
912 isotopic general circulation models to improve hydrological modeling in large  
913 mountainous catchments on the Tibetan Plateau?, *Hydrology and Earth System Sciences*,  
914 25, 6151-6172, 10.5194/hess-25-6151-2021, 2021a.

915 Nan, Y., He, Z., Tian, F., Wei, Z., and Tian, L.: Assessing the influence of water sampling  
916 strategy on the performance of tracer-aided hydrological modeling in a mountainous basin  
917 on the Tibetan Plateau, *Hydrology and Earth System Sciences*, 26, 4147-4167,  
918 10.5194/hess-26-4147-2022, 2022.

919 Nan, Y., Tian, L., He, Z., Tian, F., and Shao, L.: The value of water isotope data on improving  
920 process understanding in a glacierized catchment on the Tibetan Plateau, *Hydrology and  
921 Earth System Sciences*, 25, 3653-3673, 10.5194/hess-25-3653-2021, 2021b.

922 Olsson, T., Jakkila, J., Veijalainen, N., Backman, L., Kaurola, J., and Vehvilainen, B.: Impacts  
923 of climate change on temperature, precipitation and hydrology in Finland - studies using

924 bias corrected Regional Climate Model data, *Hydrology and Earth System Sciences*, 19,  
925 3217-3238, 10.5194/hess-19-3217-2015, 2015.

926 Piani, C., Weedon, G. P., Best, M., Gomes, S. M., Viterbo, P., Hagemann, S., and Haerter, J. O.:  
927 Statistical bias correction of global simulated daily precipitation and temperature for the  
928 application of hydrological models, *Journal of Hydrology*, 395, 199-215,  
929 10.1016/j.jhydrol.2010.10.024, 2010.

930 Rasouli, K., Pomeroy, J. W., and Marks, D. G.: Snowpack sensitivity to perturbed climate in a  
931 cool mid-latitude mountain catchment, *Hydrological Processes*, 29, 3925-3940,  
932 10.1002/hyp.10587, 2015.

933 Rasouli, K., Pomeroy, J. W., Janowicz, J. R., Carey, S. K., and Williams, T. J.: Hydrological  
934 sensitivity of a northern mountain basin to climate change, *Hydrological Processes*, 28,  
935 4191-4208, 10.1002/hyp.10244, 2014.

936 Reggiani, P., Hassanizadeh, S. M., Sivapalan, M., and Gray, W. G.: A unifying framework for  
937 watershed thermodynamics: constitutive relationships, *Advances in Water Resources*, 23,  
938 15-39, 10.1016/s0309-1708(99)00005-6, 1999.

939 Schaepli, B. and Gupta, H. V.: Do Nash values have value?, *Hydrological Processes*, 21, 99-  
940 104, 2007.

941 Schaepli, B., Hingray, B., Niggli, M., and Musy, A.: A conceptual glacio-hydrological model  
942 for high mountainous catchments, *Hydrology and Earth System Sciences*, 9, 95-109,  
943 10.5194/hess-9-95-2005, 2005.

944 Stadnyk, T. A. and Holmes, T. L.: Large scale hydrologic and tracer aided modelling: A review,  
945 *Journal of Hydrology*, 618, 10.1016/j.jhydrol.2023.129177, 2023.

946 Su, T., Miao, C. Y., Duan, Q. Y., Gou, J. J., Guo, X. Y., and Zhao, X.: Hydrological response to  
947 climate change and human activities in the Three-River Source Region, *Hydrology and*  
948 *Earth System Sciences*, 27, 1477-1492, 10.5194/hess-27-1477-2023, 2023.

949 Tang, Q. H., Lan, C., Su, F. G., Liu, X. C., Sun, H., Ding, J., Wang, L., Leng, G. Y., Zhang, Y.  
950 Q., Sang, Y. F., Fang, H. Y., Zhang, S. F., Han, D. M., Liu, X. M., He, L., Xu, X. M., Tang,  
951 Y., and Chen, D. L.: Streamflow change on the Qinghai-Tibet Plateau and its impacts,  
952 *Chinese Science Bulletin-Chinese*, 64, 2807-2821, 10.1360/tb-2019-0141, 2019.

953 Tian, F., Hu, H., Lei, Z., and Sivapalan, M.: Extension of the Representative Elementary

954 Watershed approach for cold regions via explicit treatment of energy related processes,  
955 Hydrology and Earth System Sciences, 10, 619-644, 10.5194/hess-10-619-2006, 2006.

956 Tian, F., Xu, R., Nan, Y., Li, K., and He, Z.: Quantification of runoff components in the Yarlung  
957 Tsangpo River using a distributed hydrological model, *Advances in Water Science*, 31,  
958 324-336, 2020.

959 Tong, R., Parajka, J., Salentinig, A., Pfeil, I., Komma, J., Szeles, B., Kuban, M., Valent, P.,  
960 Vreugdenhil, M., Wagner, W., and Bloeschl, G.: The value of ASCAT soil moisture and  
961 MODIS snow cover data for calibrating a conceptual hydrologic model, *Hydrology and*  
962 *Earth System Sciences*, 25, 1389-1410, 10.5194/hess-25-1389-2021, 2021.

963 van Pelt, S. C., Kabat, P., ter Maat, H. W., van den Hurk, B., and Weerts, A. H.: Discharge  
964 simulations performed with a hydrological model using bias corrected regional climate  
965 model input, *Hydrology and Earth System Sciences*, 13, 2387-2397, 10.5194/hess-13-  
966 2387-2009, 2009.

967 van Pelt, S. C., Kabat, P., ter Maat, H. W., van den Hurk, B. J. J. M., and Weerts, A. H.:  
968 Discharge simulations performed with a hydrological model using bias corrected regional  
969 climate model input, *Hydrology and Earth System Sciences*, 13, 2387-2397, 10.5194/hess-  
970 13-2387-2009, 2009.

971 Wang, S., Liu, J., Pritchard, H. D., Ke, L., Qiao, X., Zhang, J., Xiao, W., and Zhou, Y.:  
972 Characterizing 4 decades of accelerated glacial mass loss in the west Nyainqentanglha  
973 Range of the Tibetan Plateau, *Hydrology and Earth System Sciences*, 27, 933-952,  
974 10.5194/hess-27-933-2023, 2023.

975 Wang, T., Zhao, Y. T., Xu, C. Y., Ciais, P., Liu, D., Yang, H., Piao, S. L., and Yao, T. D.:  
976 Atmospheric dynamic constraints on Tibetan Plateau freshwater under Paris climate  
977 targets, *Nature Climate Change*, 11, 10.1038/s41558-020-00974-8, 2021.

978 Wang, Y. W., Wang, L., Zhou, J., Yao, T. D., Yang, W., Zhong, X. Y., Liu, R. S., Hu, Z. D., Luo,  
979 L., Ye, Q. H., Chen, N. S., and Ding, H. T.: Vanishing Glaciers at Southeast Tibetan Plateau  
980 Have Not Offset the Declining Runoff at Yarlung Zangbo, *Geophysical Research Letters*,  
981 48, 10.1029/2021gl094651, 2021.

982 Wang, L., Han, S., Tian, F., Li, K., Li, Y., Tudaji, M., Cao, X., Nan, Y., Cui, T., Zheng, X., Hu,  
983 Z., Wang, W., and Yang, Y.: The Evaporation on the Tibetan Plateau Stops Increasing in



984 the Recent Two Decades, *Journal of Geophysical Research-Atmospheres*, 127,  
985 10.1029/2022jd037377, 2022.

986 Wang, L., Yao, T. D., Chai, C. H., Cuo, L., Su, F. G., Zhang, F., Yao, Z. J., Zhang, Y. S., Li, X.  
987 P., Qi, J., Hu, Z. D., Liu, J. S., and Wang, Y. W.: TP-River: Monitoring and Quantifying  
988 Total River Runoff from the Third Pole, *Bulletin of the American Meteorological Society*,  
989 102, E948-E965, 10.1175/bams-d-20-0207.1, 2021.

990 Wu, Y., Long, D., Lall, U., Scanlon, B. R., Tian, F., Fu, X., Zhao, J., Zhang, J., Wang, H., and  
991 Hu, C.: Reconstructed eight-century streamflow in the Tibetan Plateau reveals contrasting  
992 regional variability and strong nonstationarity, *Nature Communications*, 13,  
993 10.1038/s41467-022-34221-9, 2022.

994 Xu, R., Hu, H. C., Tian, F. Q., Li, C., and Khan, M. Y. A.: Projected climate change impacts on  
995 future streamflow of the Yarlung Tsangpo-Brahmaputra River, *Global and Planetary  
996 Change*, 175, 144-159, 10.1016/j.gloplacha.2019.01.012, 2019.

997 Xu, R., Tian, F., Yang, L., Hu, H., Lu, H., and Hou, A.: Ground validation of GPM IMERG and  
998 TRMM 3B42V7 rainfall products over southern Tibetan Plateau based on a high-density  
999 rain gauge network, *Journal of Geophysical Research-Atmospheres*, 122, 910-924,  
1000 10.1002/2016jd025418, 2017.

1001 Yang, K. and He, J.: China meteorological forcing dataset (1979–2018), National Tibetan  
1002 Plateau Data Center [dataset], 10.11888/AtmosphericPhysics.tpe.249369.file, 2019.

1003 Yao, T. D.: Tackling on environmental changes in Tibetan Plateau with focus on water,  
1004 ecosystem and adaptation, *Science Bulletin*, 64, 417-417, 10.1016/j.scib.2019.03.033,  
1005 2019.

1006 Yao, Y. Y., Zheng, C. M., Andrews, C. B., Scanlon, B. R., Kuang, X. X., Zeng, Z. Z., Jeong, S.  
1007 J., Lancia, M., Wu, Y. P., and Li, G. S.: Role of Groundwater in Sustaining Northern  
1008 Himalayan Rivers, *Geophysical Research Letters*, 48, 10.1029/2020gl092354, 2021.

1009 Yao, T. D., Bolch, T., Chen, D. L., Gao, J., Immerzeel, W., Piao, S., Su, F. G., Thompson, L.,  
1010 Wada, Y., Wang, L., Wang, T., Wu, G. J., Xu, B. Q., Yang, W., Zhang, G. Q., and Zhao, P.:  
1011 The imbalance of the Asian water tower, *Nature Reviews Earth & Environment*, 3, 618-  
1012 632, 10.1038/s43017-022-00299-4, 2022.

1013 Yoshimura, K., Kanamitsu, M., Noone, D., and Oki, T.: Historical isotope simulation using

1014 Reanalysis atmospheric data, *Journal of Geophysical Research-Atmospheres*, 113,  
1015 10.1029/2008jd010074, 2008.

1016 Zhang, T., Li, D., East, A. E., Walling, D. E., Lane, S., Overeem, I., Beylich, A. A., Koppes, M.,  
1017 and Lu, X.: Warming-driven erosion and sediment transport in cold regions, *Nature*  
1018 *Reviews Earth & Environment*, 3, 832-851, 10.1038/s43017-022-00362-0, 2022a.

1019 Zhang, T., Li, D. F., and Lu, X. X.: Response of runoff components to climate change in the  
1020 source-region of the Yellow River on the Tibetan plateau, *Hydrological Processes*, 36,  
1021 10.1002/hyp.14633, 2022b.

1022 Zhang, F., Zhang, H. B., Hagen, S. C., Ye, M., Wang, D. B., Gui, D. W., Zeng, C., Tian, L. D.,  
1023 and Liu, J. S.: Snow cover and runoff modelling in a high mountain catchment with scarce  
1024 data: effects of temperature and precipitation parameters, *Hydrological Processes*, 29, 52-  
1025 65, 10.1002/hyp.10125, 2015.

1026 Zhao, Q., Ding, Y., Wang, J., Gao, H., Zhang, S., Zhao, C., Xu, J., Han, H., and Shanguan, D.:  
1027 Projecting climate change impacts on hydrological processes on the Tibetan Plateau with  
1028 model calibration against the glacier inventory data and observed streamflow, *Journal of*  
1029 *Hydrology*, 573, 60-81, 10.1016/j.jhydrol.2019.03.043, 2019.